J. Fluid Mech. (1972), *vol.* 51, *part* 2, *pp.* 301–335
Printed in Great Britain

Fully developed asymmetric flow in a plane channel

By K. HANJALIĆ
Mašinski fakultet, Sarajevo, Jugoslavia
AND B. E. LAUNDER
Imperial College, London

(Received 3 March 1971)

The paper presents the results of a detailed experimental examination of fully developed asymmetric flow between parallel planes. The asymmetry was introduced by roughening one of the planes while the other was left smooth; the ratio of the shear stresses at the two surfaces was typically about 4:1.

The main emphasis of the research has been on establishing the turbulence structure, particularly in the central region of the channel where the two dissimilar wall flows (generated by the smooth and rough surfaces) interact. Measurements have included profiles of all non-zero double and triple velocity correlations; spectra of the same correlations at several positions in the channel; skewness and flatness factors; and lateral two-point space correlations of the streamwise velocity fluctuation.

The region of greatest interaction is characterized by strong diffusional transport of turbulent shear stress and kinetic energy from the rough towards the smooth wall region, giving rise, *inter alia*, to an appreciable separation between the planes of zero shear stress and maximum mean velocity. The profiles of length scales of the larger-scale motion are, in contrast to the turbulent velocity field, nearly symmetric. Moreover, it appears that at high Reynolds numbers the small-scale motion may in many respects be treated as isotropic.

1. Introduction

Detailed experimental examination of the structure of turbulent shear flows has, for the most part, been concerned with comparatively simple flows. In internal flows, for example, a number of workers have made detailed turbulence measurements of fully developed flow in a circular-sectioned pipe and in a plane symmetric channel (Laufer 1951, 1954; Comte-Bellot 1965; Coantic 1967; Clark 1968; Van Thinh 1967) but, until recently, no studies of equivalent depth had been made in ducts of more complex geometry. This focusing of attention on symmetric flows was natural since some of the features of the turbulent motion could most readily be discerned if the influence of others was absent or small.

Practically important flows through ducts, however, do not commonly possess this simplifying feature. It may therefore be expected that any mathematical model of turbulence formulated with reference to existing experimental data for symmetric flows would exhibit deficiencies when used to predict more complex flows. It thus appeared desirable to undertake a thorough examination of the

turbulence structure in a flow which, in at least one respect, was substantially more complicated than those which had hitherto attracted attention.

The geometry selected for the present study was a rectangular duct of sufficiently large aspect ratio for the flow along the mid-plane to be considered as that developed between infinite parallel planes. Asymmetry was introduced by roughening one of the principal sides of the duct while the opposite surface was left smooth. Except for some preliminary tests, all measurements were made far enough downstream for the flow to have become fully developed. Thus all turbulence and mean flow profiles were functions only of the distance co-ordinate normal to the plates, denoted here by x_2 or $\tilde{x}_2$ according to whether the smooth or the rough surface is taken as the co-ordinate origin.

In an interim report (Hanjalić & Launder 1968), the authors demonstrated that the mean velocity distribution between the plates exhibited three distinct regimes. In the vicinity of each of the walls, the velocity profile displayed the universal variation appropriate to each surface. That is to say, near the smooth wall, the profile was in good accord with the logarithmic 'law of the wall'

$$u_S^+ = (1/\kappa)\ln x_{2_S}^+ + c \tag{1.1}$$

and correspondingly, near the rough wall, the variation was well described by

$$u_R^+ = (1/\kappa)\ln(x_2/e) + c'. \tag{1.2}$$

In the above equations, u^+ stands for the local streamwise velocity U_1, normalized by the friction velocity, $(\tau_w/\rho)^{\frac{1}{2}}$, and the subscripts S and R denote respectively whether the rough or smooth wall shear stress, τ_{w_R} or τ_{w_S}, is used in the friction velocity. For the latter equation, e denotes a characteristic height of the roughness and c' is a constant independent of Reynolds number.

The conformity of the near-wall profiles with the above equations indicated that the flow there was essentially in local equilibrium and unaware of the dissimilar structure prevailing near the opposite walls. In the central region of the channel, however, the mean flow displayed evidence of strong interaction between the two wall regions. A striking feature of this interaction was that stationary values of mean velocity gradient and zero shear stress were non-coincident – the plane of zero shear stress lying substantially nearer the smooth wall than the plane of maximum velocity. This same phenomenon has been observed by a number of other workers: in flow through annuli by Kjellstrom & Hedberg (1968) and Lawn (1970); in wall jets by Tailland & Mathieu (1967); and in an asymmetric plane jet by Beguier (1965).† A common feature of all the above situations was that the flows in question were strongly asymmetric with respect to the surface of the zero shear stress.

For a fully developed flow, the non-coincidence of the surfaces of zero shear stress and mean rate of strain means that, over a portion of the flow, the production of turbulent kinetic energy (which arises exclusively from the working of

† A referee has pointed out that a further asymmetric flow which has received attention is that where a gas flows between a wall and a moving liquid surface, e.g. Hanratty & Engen (1957). Another referee has drawn our attention to a substantially earlier work on wall jets by Mathieu (1961) wherein the non-coincidence of the planes of zero stress and mean rate of strain was reported.

the Reynolds shear stresses against the mean velocity gradient) is negative; that is, locally there is a loss of turbulence energy to the mean motion. This phenomenon leads to particular interest in the turbulence energy balance in such flows and it is a subject to which attention is paid here. The measurements reported include profiles of all non-zero double- and triple-velocity correlations and, with only one exception, their one-dimensional spectra as well. From these data, representative length scales have been deduced for both the macro and micro structure of the turbulence and these are compared with the integral length scale deduced from two-point velocity correlations.

2. Apparatus and instrumentation

Apparatus

The test section, shown schematically in figure 1, was formed of two 9·6 mm thick 'Duralumin' plates mounted vertically with two aluminium channel-section spacers used as the closing top and bottom walls of the channel. One of

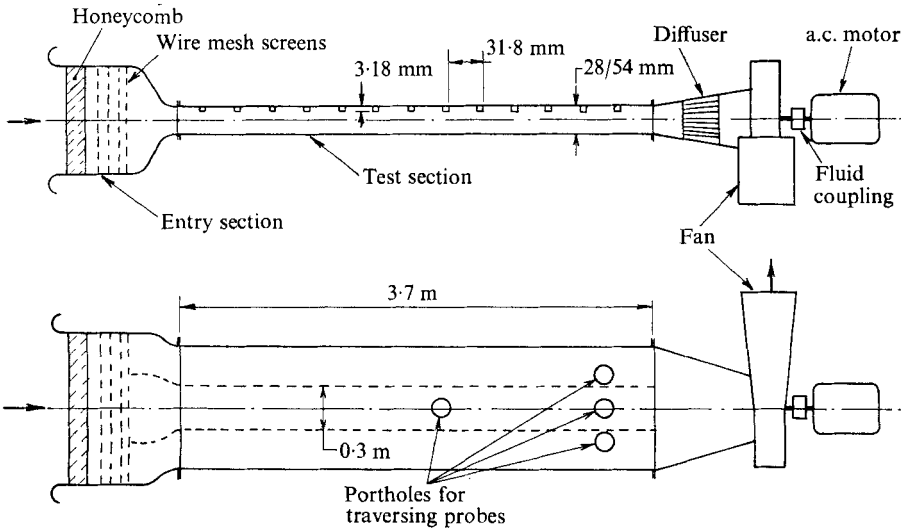

FIGURE 1. Schematic view of wind tunnel.

the side walls was roughened by sticking 3·18 mm square-sectioned silver steel ribs (transverse to the flow direction) spaced to give a pitch-to-height ratio of 10:1. Two channel widths have been considered, 28 and 54 mm measured between the smooth wall and the root of the ribs. The distance between the top and bottom walls was 0·3 m; the aspect ratio was thus about 12:1 for the narrower duct and 6:1 for the wider. The total channel length was 3·70 m.

Static pressure holes, 0·4 mm diameter, were inserted at 0·15 m intervals along the centre-line of each test plate; the static pressures were recorded on a T.E.M. multi-limb manometer. The downstream smooth-wall plate was fitted with access port-holes 76 mm in diameter (see figure 1) for examining the flow. Apart from preliminary readings to ascertain that the flow was fully developed, all measurements were taken at the downstream centre-line port-hole.

Air was drawn through the test section by a centrifugal fan driven by a 15 h.p. a.c. motor through a Vulcan fluid coupling thus enabling the flow rate to be varied by a factor of about 5.

Instrumentation

Mean velocity profiles across the test-section were measured by means of flattened-tip Pitot tubes with internal and external tip heights of 0·15 mm and 0·45 mm respectively. The width of these tubes at the tip was about 2·5 mm. Different Pitot tubes were used for examining the flow near each of the walls and these were suitably shaped to enable contact to be made with the surface in question. The probes gave consistent readings in the central region of the channel accessible to both of them.

In determining the mean velocity profiles, MacMillan's (1954, 1956) low-Reynolds-number and shear displacement corrections were applied to the Pitot tube measurements.† Moreover, it was supposed that the Pitot tube responded only to the longitudinal component of turbulence. To determine the position of maximum velocity, a calibrated double Pitot tube was employed consisting of two flattened tipped tubes with centres 1 mm apart.

Stanton and Preston tubes were used as the basis for determining the smooth-wall shear stress. The Preston tube was made from 0·8 mm O.D. stainless-steel tubing and the Stanton tube from a Schick single-edged razor blade stuck to the surface with Araldite. Both probes were mounted on aluminium disks 76 mm in diameter which fitted flush into the access port-holes in the smooth plate. The tubes were calibrated in fully developed flow between two smooth plates.

Hot-wire measurements

Standard Disa miniature hot-wire probes and constant-temperature anemometers were employed for the turbulence measurements. Two 55D01 anemometers, in conjunction with 55D10 linearizers, a 55D35 r.m.s. voltmeter and a Solartron d.c. digital voltmeter, were employed for this purpose. The longitudinal turbulence components were measured with the gold-plated boundary-layer-type probe 55F04, while for the measurements of the lateral components and turbulent shear stress, the miniature X-wire probe, type 55A38, was used.

Calibration of the hot wire was performed before and after each run in a nearby boundary-layer wind tunnel. A number of values of the linearizer exponent setting (the reciprocal of the exponent in the Collis & Williams (1959) law) were tried initially, ranging from 2·0 to 2·5; a value of 2·25 was finally adopted. The wires of the X-probe showed nearly equal sensitivities and the small discrepancy was reduced even further by adjustment to the zero velocity voltage and to the gain of one of the linearizers. No correction for possible wire interference was attempted.

For the X-probes, the effective cooling velocity was assumed in the form proposed by Champagne, Sleicher & Wehrmass (1967). The coefficient, representing the fraction of the velocity component parallel to the wire that affects the wire

† MacMillan's proposals were for Pitot tubes of circular cross-section; their use for flattened tubes has, however, been found by Escudier (1967) to improve the universality of the near-wall velocity profile.

cooling, was assigned the value of 0·23 for the considered velocity range and wire length: diameter ratio of 200: 1; this practice accords with the recommendations of Champagne *et al.* (1967), Kjellstrom & Hedberg (1968) and Lawn (1970). The two fluctuating signals were correlated by means of the Disa 55D75 and Disa 55A06 correlators. The latter was employed during the measurements of the triple velocity correlations, when the squaring circuit of the 55D75 correlator was utilized for squaring one of the fluctuating signals. The turbulent shear stress and the triple correlations of u_1 and u_2 were determined by measuring the correlation coefficients and the r.m.s. values of the relevant components. The measurements of the triple correlation $\overline{u_3^2 u_2}$ were performed by placing the X-wire probe in a plane bisecting the x_1, x_3 and x_2, x_3 planes.

Of the quadruple correlations, only the flatness factors of the probability distribution of u_1 and u_2 were considered. These were evaluated indirectly from the r.m.s. of the fluctuating part of the squared signal (Hanjalić 1970).

For the measurements of frequency spectra, two equal Brüel & Kjaer audio-frequency spectrometers, type 2112, were employed. The spectrometers have a selective frequency range of 22–45000 Hz, containing 33 filters with bandwidth of one-third octave and 11 filters with one octave bandwidth.

The multiplication of the filtered fluctuating signals for the measurements of the triple velocity spectra was performed by means of an analog multiplier with a flat frequency response up to 250 kHz (-3 db) and a phase error of 1 % at 3 kHz (Analog Devices type 421K).

Several possible corrections to the hot-wire readings were considered, but none appeared to have a significant effect. The maximum error due to the neglect of the second-order terms in the non-linear hot-wire response equations was about 5·5 % for the measurements with the X-probe in the x_1, x_2 plane at the nearest position to the rough wall. The error decreased rapidly with increasing distance from the wall; for the X-probe in the x_1, x_3 plane and for the normal probe the correction was even smaller. Frenkiel's (1956) proposed correction of the turbulence intensities to compensate for inadequate hot-wire response to the small-scale motion was negligible everywhere except very close to the smooth wall where it amounted to about 4 %.

Another form of wire-length correction for spectra measurements proposed by Wyngaard (1968) suggested that, at the highest frequency measured, the normal-wire data may have been in error by 16 %. It would appear that for the cross-wire measurements the error may have been somewhat larger; no corrections have been applied to the data, however, for our wire separation did not correspond to either of the cases examined by Wyngaard.

Traversing mechanism

The sensing probes were propelled between the test plates by means of a traversing instrument. A 50 mm micrometer was mounted on two steel guide rods cemented with Araldite into a 76 mm aluminium disk; the disk itself was clamped flush with the test plate in the access port-holes. For the measurements of space correlations employing two probes, a similar design of traversing instrument was used but with two pairs of guide rods and two micrometers.

A simple electric circuit enabled the micrometer reading, when the probe touched the wall, to be accurately determined. When assembled in the test section the probes were not visible and so, to enable accurate positioning of the hot-wire probes, a dummy test plate, made from the same plate as the channel walls, was employed. At several micrometer readings the actual distances of the hot wire from the dummy plate were measured with a travelling microscope. Moreover, following the proposals of Zaric (1967) zero velocity voltage readings of the hot wire were recorded as a function of the distance from the dummy wall, yielding an exponential curve which served then as a reference for the actual positioning of the hot-wire probe when placed in the channel. The latter method served as a check on possible misalignment of the disk's inner surface with the surface of the channel wall in comparison with the surface of the dummy plate. The correction never exceeded 0·05 mm.

Preliminary tests

The apparatus was first assembled with two smooth test plates 1·85 m long 25 mm apart. For a number of Reynolds numbers, measurements of the mean velocity profile were made with the Pitot tubes. The profiles were plotted semi-

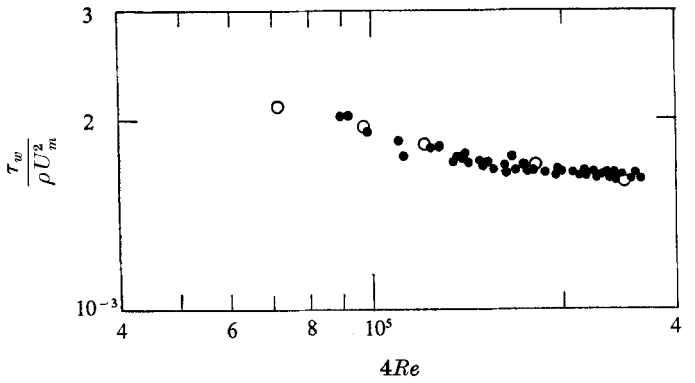

FIGURE 2. Friction factor in plane symmetric channel: ○, from equation (1.1); ●, from measured static pressure gradient.

logarithmically and the value of the wall shear stress deduced in the usual way from the application of equation (1.1) to the linear region of the profile. Two pairs of values of the constants κ and c were used: $\kappa = 0{\cdot}41$, $c = 5{\cdot}0$ (Coles's (1962) recommendation) and $\kappa = 0{\cdot}42$, $c = 5{\cdot}45$ (suggested by Patel (1965)). Over the range of Reynolds numbers used here, the two sets of constants gave rise to differences in the deduced values of τ_w of only about 1 %.

A more extensive set of readings was taken in which only the maximum velocity, the static pressure gradient and the Stanton- and Preston-tube readings were recorded. The wall shear stress was deduced from the linear portion of the static pressure distribution; then, with the maximum channel velocity measured, the skin-friction coefficients could be deduced. The skin-friction coefficients deduced from both the static pressure gradient and equation (1.1) are plotted as a function of Reynolds number in figure 2. The values deduced by the two methods

are seen to be in satisfactory agreement. Thus it was deduced that the apparatus was functioning satisfactorily.

A least-mean-square fit to the Stanton-tube readings yielded the following correlation:

$$\left(\frac{\tau_w \rho d^2}{\mu^2}\right) = 0{\cdot}326 \left(\frac{\Delta P_{St} \rho d^2}{\mu^2}\right)^{0{\cdot}76},$$

where ΔP_{St} refers to the dynamic pressure recorded by the Stanton tube and where d is the distance from the aluminium disk to the cutting edge of the blades. This correlation was found to be consistently reproducible. The shear stress of the smooth wall in the rough–smooth channel obtained from this equation was always within 2 % of the values indicated by equation (1.1) and agreed within 3 % with the values obtained from Preston-tube data employing the Head & Rechenberg (1962) correlation. The Stanton-tube values for the smooth wall shear stress have been adopted throughout this work as the standard ones.

3. Mean flow characteristics

Figure 3 shows the distribution of mean velocity between the rough–smooth parallel planes for three values of Reynolds number, where Re is based upon the maximum velocity and half the distance between the plates. The profiles are strongly asymmetric and are appreciably dependent upon Reynolds number. This Reynolds-number influence may be attributed to the fact that the ratio $\tau_R : \tau_S$ increases approximately as $U_{\max}^{\frac{1}{2}}$. Although, as figure 3 reveals, the surfaces of zero shear stress and maximum velocity do not coincide, one would expect a shift in one of them to be accompanied by a similar displacement of the other.

The mean velocity profiles near the smooth surface are plotted in figure 4 in universal co-ordinates; the shear stress used in determining u_S^+ and x_2^+ is that found from the Stanton-tube measurements. If one discounts the scatter in the data for $x_2^+ < 50$ (which may reasonably be attributed to uncertainties in estimating the displacement correction of the Pitot tube), it is evident that, for an appreciable region near the wall, the mean velocity profile is universal in character, there being no detectable influences either of Reynolds number or of the rough surface opposite. The findings, with respect to the influence of Reynolds number, do not accord with those of Clark (1968) and Comte-Bellot (1965) in smooth channels. These workers noted appreciable changes in the additive constant of the logarithmic profile with Reynolds number though, as figure 4 shows, the trends were opposite in the two sets of experiments. Of the plane-channel data, the present measurements agree most closely with Comte-Bellot's profile at a Reynolds number of 120000; Patel's (1965) recommended logarithmic law, however, provides an even better fit. Further from the surface, as the influence of the rough wall progressively increases, the mean velocity profile departs *below* the logarithmic profile in contrast to the departure above the logarithmic profile found in a symmetric smooth channel.

The velocity profiles near the rough wall are shown in figure 5 for three Reynolds numbers, the normalizing scales being the rough-wall friction velocity and the rib height, e. The left-hand graph reveals that there is no detectable

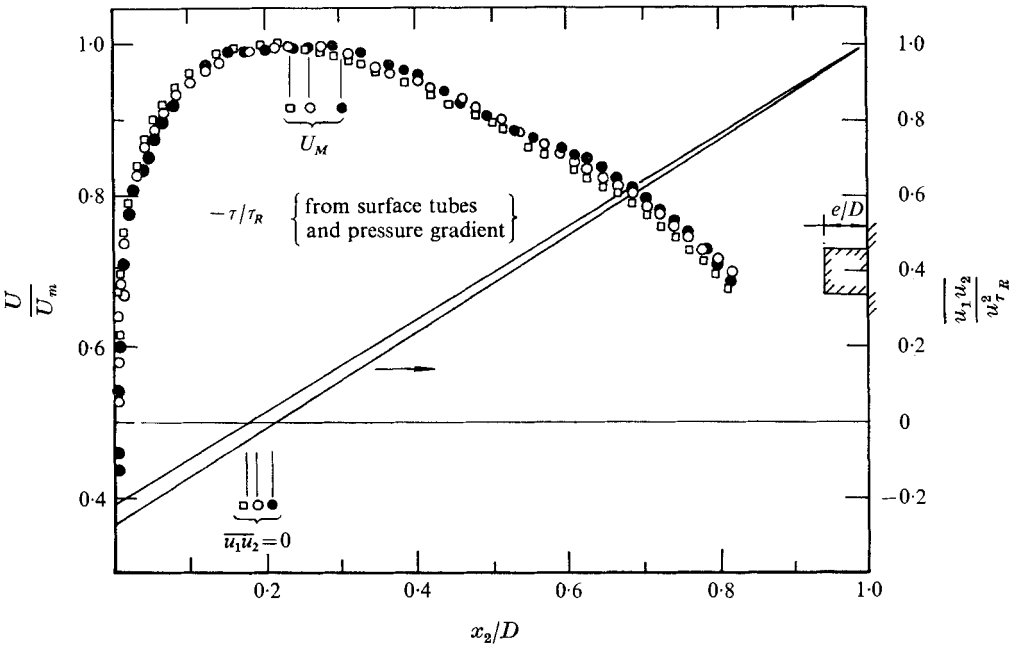

FIGURE 3. Mean velocity profiles in 54 mm asymmetric channel. ●, Re = 18 700; ○, Re = 36 400; □, Re = 56 000.

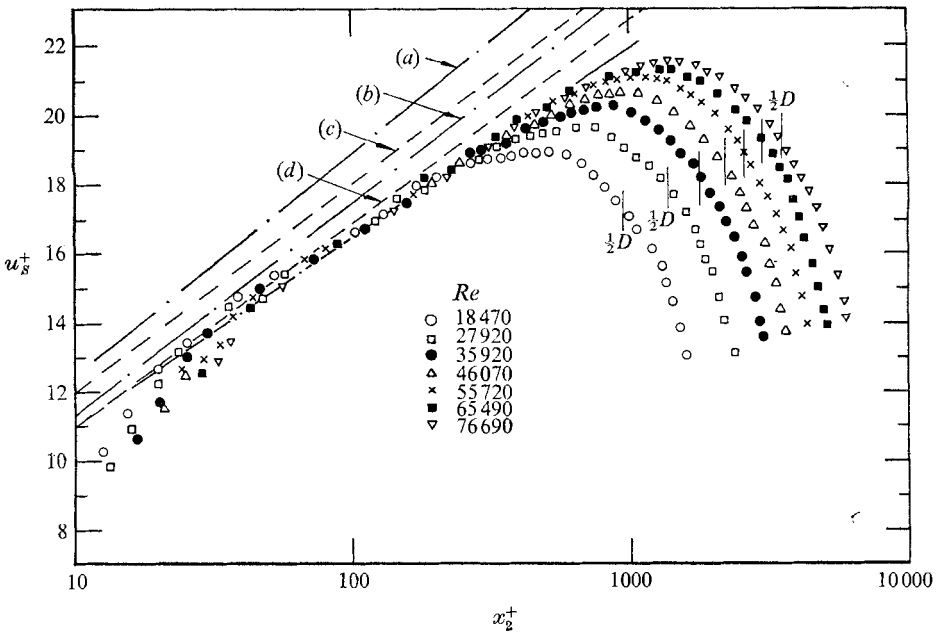

FIGURE 4. Smooth-wall velocity profiles in universal co-ordinates, 54 mm channel. ——, Patel (1965); ·——·, Clark (1968): (*a*) Re = 68000, (*b*) Re = 14700; – – – – –, Comte-Bellot (1965): (*c*) Re = 570000, (*d*) Re = 120000.

influence of Reynolds number and, over a region extending from about 5 to 8 rib heights, the profiles display a logarithmic variation with the same slope as the smooth-wall region (i.e. $\kappa = 0{\cdot}42$). Perry & Joubert (1963) found, for surfaces roughened with discrete ribs, that the effective origin for $\tilde{x}_2$ may not coincide with the root of the rib. The same conclusion emerges from the present work; for as figure 5(*b*) displays, if the origin is taken as 0·4 rib heights below the root of the rib, all the profiles collapse onto the logarithmic line at distances greater than two rib heights from this new origin. The additive constant in the logarithmic law, 3·2, is in reasonable agreement with the data of Wilkie *et al.* (1967) for a similar type of roughness.

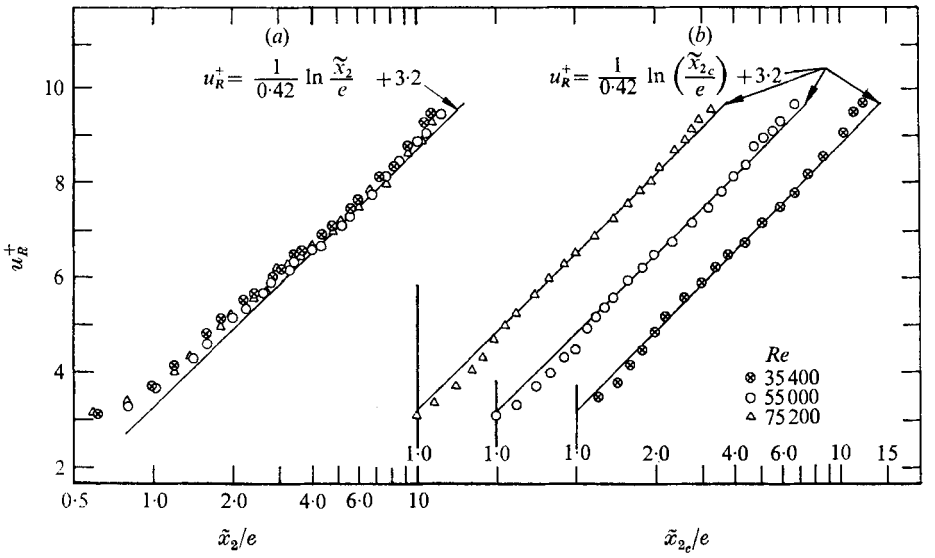

FIGURE 5. Rough-wall velocity profiles, 54 mm channel.

Figure 3 indicated that the planes of maximum velocity and zero shear stress are not coincident in this asymmetric channel flow. Figure 6, which provides results for the 54 and 28 mm channels, permits a more detailed appraisal of this phenomenon. The position of zero stress, y_0, lies significantly closer to the smooth surface than that of maximum velocity, y_m, the discrepancy being larger for the 28 mm channel where the ratio $e:D$ is greater. Both the maximum-velocity and zero-stress positions shift progressively towards the smooth surface as the Reynolds number is increased. The ratio $y_0:y_m$ does not, however, vary appreciably for either duct over the range of these experiments.

In summary, close to the smooth wall and over a considerable region near the rough wall, the mean velocity field shows evidence of local equilibrium; there the mean velocity profiles are universal when normalized with length and velocity scales appropriate to the region in question. Within a central region of the channel, however, the local flow structure is markedly influenced by the dissimilar boundaries. The sections which follow provide a detailed examination of the turbulence single-point double and triple correlations within these flow regimes.

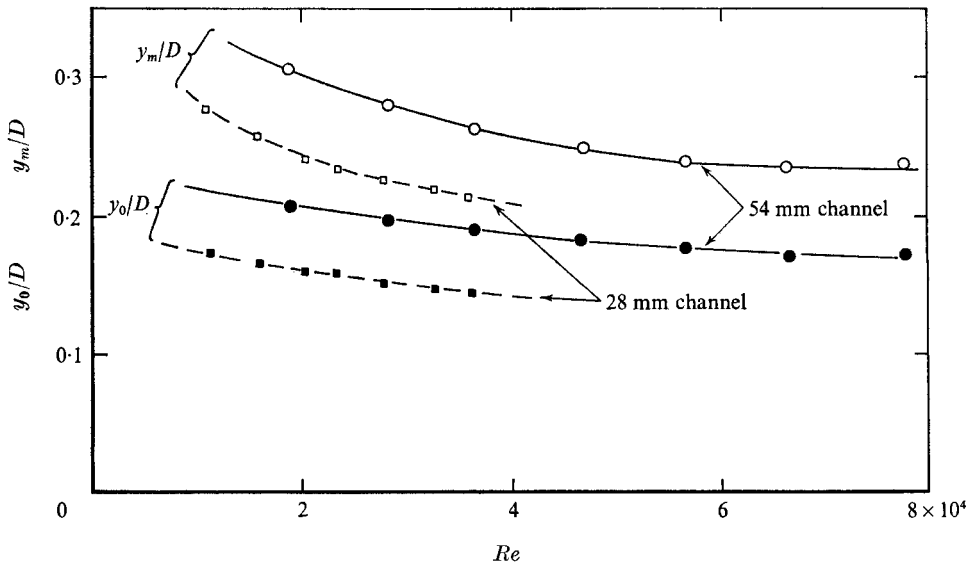

FIGURE 6. Variation of y_m and y_0 with Reynolds number.

4. Profiles of single-point turbulence correlations

The distribution of all three components of the r.m.s. turbulence intensity are shown in figure 7 for three Reynolds numbers. The axes are normalized with the rough-wall friction velocity and the distance from the rough surface to the plane of zero shear stress, $\tilde{y}_0$. It is noted that the profiles shown for $\tilde{u}_1$ are those obtained from a cross-wire placed in the x_1, x_3 plane. Other $\tilde{u}_1$ profiles have, however, been taken with a normal wire (for which one set of data is included in figure 7) and with a cross-wire placed in the x_1, x_2 plane; all the results were consistent within a maximum experimental scatter of 7 %. The cross-wire data are selected for presentation here because they cover a greater proportion of the channel width than was accessible to the bent-pronged normal-wire probe.

From the rough surface to almost the plane of zero shear stress, the profiles of all three turbulence intensity components show no discernible variation with Reynolds number. In view of the mean flow findings, the result accords with expectations. Some influence of the unequal boundary conditions may be detected, however, since the minimum value of $\tilde{u}_3/\tilde{u}_2$ may be seen to occur at a value of $\tilde{x}_2/\tilde{y}_0$ of approximately 0·75, whereas in a symmetric channel the minimum is at the plane of zero shear stress.

Closer to the smooth wall, for $\tilde{x}_2/\tilde{y}_0 > 0{\cdot}95$, the influence of Reynolds number becomes apparent, the intensities increasing as Re decreases. This behaviour is expected since, as the smooth surface is approached, the flow field becomes progressively under the influence of the smooth-wall scales u_{τ_S} and ν/u_{τ_S}. Since the ratio $u_{\tau_R}:u_{\tau_S}$ diminishes with a decrease in Reynolds number, this will reflect in an increase in $\tilde{u}_i/u_{\tau_R}$ if $\tilde{u}_i/u_{\tau_S}$ is independent of Reynolds number.

A noteworthy feature of the data is that the minima of the turbulence intensities do not coincide with y_0. The minimum values of $\tilde{u}_1$ and $\tilde{u}_3$ occur at approxi-

mately $0{\cdot}8\ y_0$ while, over the portion of the duct covered in these measurements, u_2 diminishes uniformly as the smooth wall is approached. Consideration of the $\tilde{u}_1$ profile in the immediate vicinity of the surface is deferred to the appendix, where critical comparison is made with other workers' data. Suffice it to mention here that we conclude that the $\tilde{u}_1$ profile in our experiments is not discernibly different from that in a smooth symmetric channel.

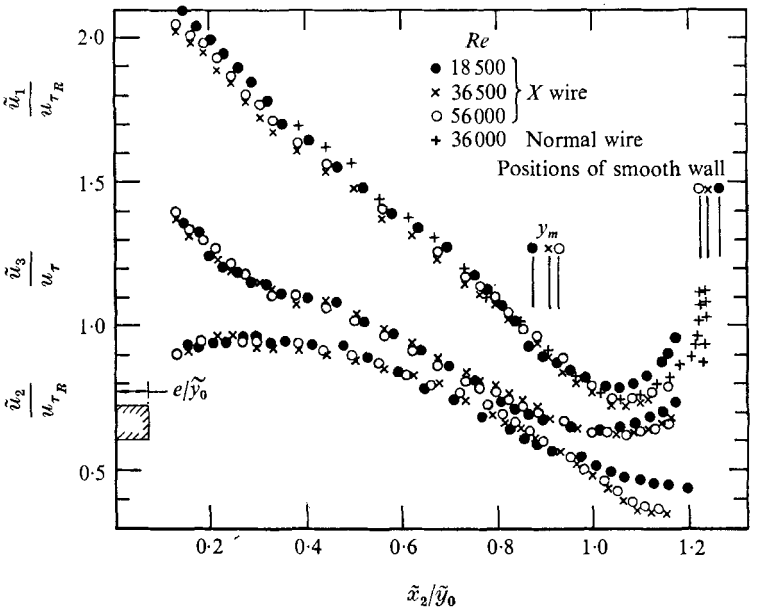

FIGURE 7. Distribution of turbulence intensities.

Figure 8 compares the measured variation of the kinematic turbulent shear stress, $\overline{u_1 u_2}$, across the channel with that deduced from the Stanton tube and static-pressure-gradient readings (indicated by the solid line). At distances greater than about four rib heights from the rough wall, the measured profiles display good linearity with a slope in accord with that implied by the static pressure gradient.† The data for the highest and lowest Reynolds number falls almost exactly on the line; those for the intermediate Reynolds number lie slightly to the right of it.

Figure 9 displays the measured variation of the shear correlation coefficient across the channel. Over a considerable region near the rough wall ($0{\cdot}1 < \tilde{x}_2/\tilde{y}_0 < 0{\cdot}65$) the correlation is practically constant and, as would be expected, there is no detectable variation with Reynolds number. The measured values for this region lie between 0·4 and 0·43 in agreement with data in smooth channels. Near the smooth wall there is no appreciable region where the correlation coefficient is uniform though the maximum value reached is again approximately 0·4.

† It is probable that the x_1 dependence of the flow in the immediate neighbourhood of the ribbed surface is responsible for much of the indicated non-linearity of the $\overline{u_1 u_2}$ profile there.

The orientation of one of the principal-stress axes is illustrated in figure 10 where the angle α_{s_1} is calculated from the expression:

$$\alpha_{s_{1,2}} = \pm \tfrac{1}{2} \tan^{-1} \left[\frac{2\overline{u_1 u_2}}{\overline{u_1^2} - \overline{u_2^2}} \right].$$

The angles of the stress axes vary considerably except over the region $0{\cdot}2 < \tilde{x}_2/\tilde{y}_0 < 0{\cdot}8$, where they are approximately 17° and −73°; these values are close to those found in the outer region of other wall flows. For comparison, it is noted that the principal axes of the mean rate of strain are orientated at ±45°; that is, the angles are constant across the channel except for an interchange between the compression and stretching axes at $x_2 = y_m$.

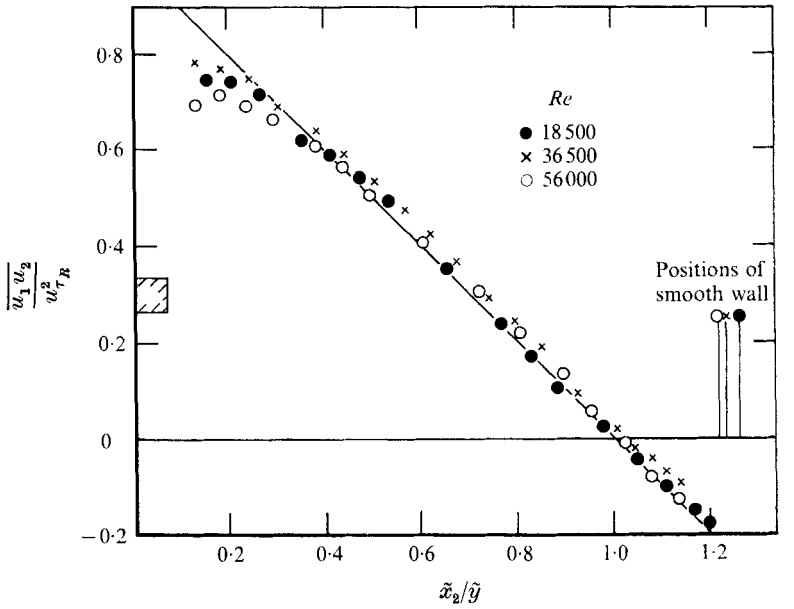

FIGURE 8. Direct measurements of $\overline{u_1 u_2}$.

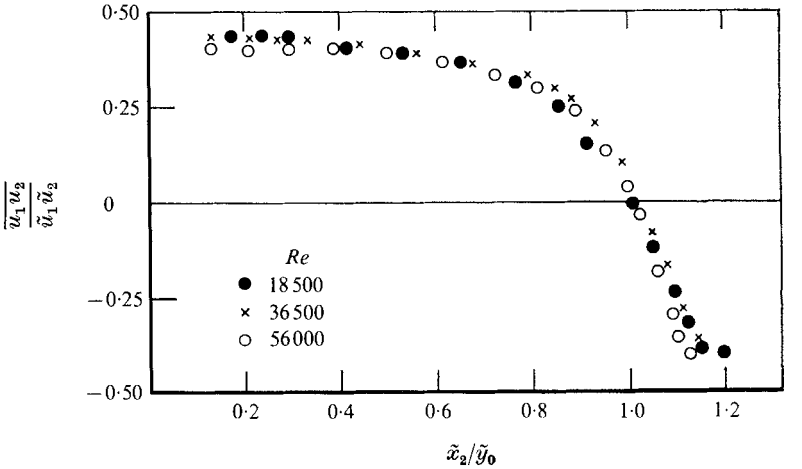

FIGURE 9. Variation of shear correlation coefficient.

The triple velocity correlations, measured at two Reynolds numbers, are presented in figures 11, 12 and 13, the normalizing scales being $u_{\tau_B}^3$ and $\tilde{y}_0$. The three energy diffusion components shown in figure 11 exhibit a sign reversal at a value of $\tilde{x}_2/\tilde{y}_0$ between 1·0 and 1·1. This is a characteristic of all velocity correlations that contain an uneven power of the u_2 component and is comparable with the change of sign of $\overline{u_1 u_2}$ near the same location. At approximately the same position the correlation $\overline{u_1 u_2^2}$, which represents the diffusion of shear stress, exhibits a minimum value (figure 12).

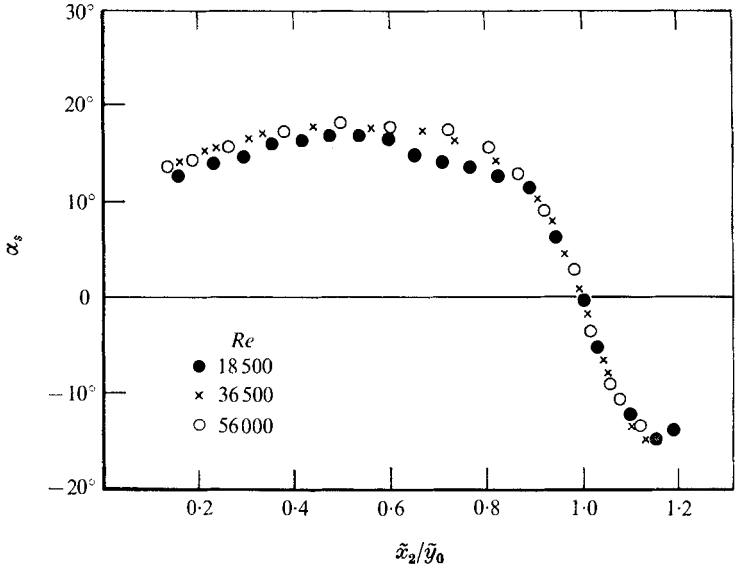

FIGURE 10. Angle of principal-stress axis with respect to x_1.

A further change of sign of the correlations $\overline{u_1^2 u_2}$, $\overline{u_2^3}$ and $\overline{u_1 u_2^2}$ is indicated near the rough wall; the trend is especially pronounced for the last of these. This behaviour (which would imply a diffusional transport of a turbulent quantity *up* the gradient of that quantity) is consistent with the shedding of large eddies (with axis in the x_3 direction) from the ribs on the rough wall. That the $\overline{u_3^2 u_2}$ component does *not* show a sign reversal lends some support to this argument, though against this must be set the fact that the energy spectra, presented in § 5, exhibit no sign of a preferred frequency. It seems probable that these measurements in the vicinity of the roughness elements are not precise enough for a definite conclusion to be drawn.

The diffusion profiles shown in figure 11 (*b*) and (*c*) and in figure 12 are noticeably different for the two Reynolds numbers. In view of the insensitivity to Reynolds number of the double correlations and the $\overline{u_1^2 u_2}$ correlation of 11 (*a*), the difference is almost certainly attributable to experimental error. It is pertinent to add that $\overline{u_2^3 u_2}$ was obtained indirectly by measuring the correlation $\overline{(u_2+u_3)^3}$ (which in a one- or two-dimensional flow is equal to $\overline{u_2^3}+\overline{3u_2^3 u_2}$) and subtracting from it the directly measured value of $\overline{u_2^3}$. Now $\overline{(u_2+u_3)^3}$ *was* essentially independent of Reynolds number and this is why the apparent effect

of Reynolds number is opposite in figures 11(*b*) and (*c*). Fortunately the error in determining $\overline{u_2^3}$ is practically eliminated when the energy diffusion, $\overline{k'u_2}$, is calculated (k' denoting the instantaneous turbulence energy). As figure 13 shows, the measurements for the two Reynolds numbers are in excellent agreement.

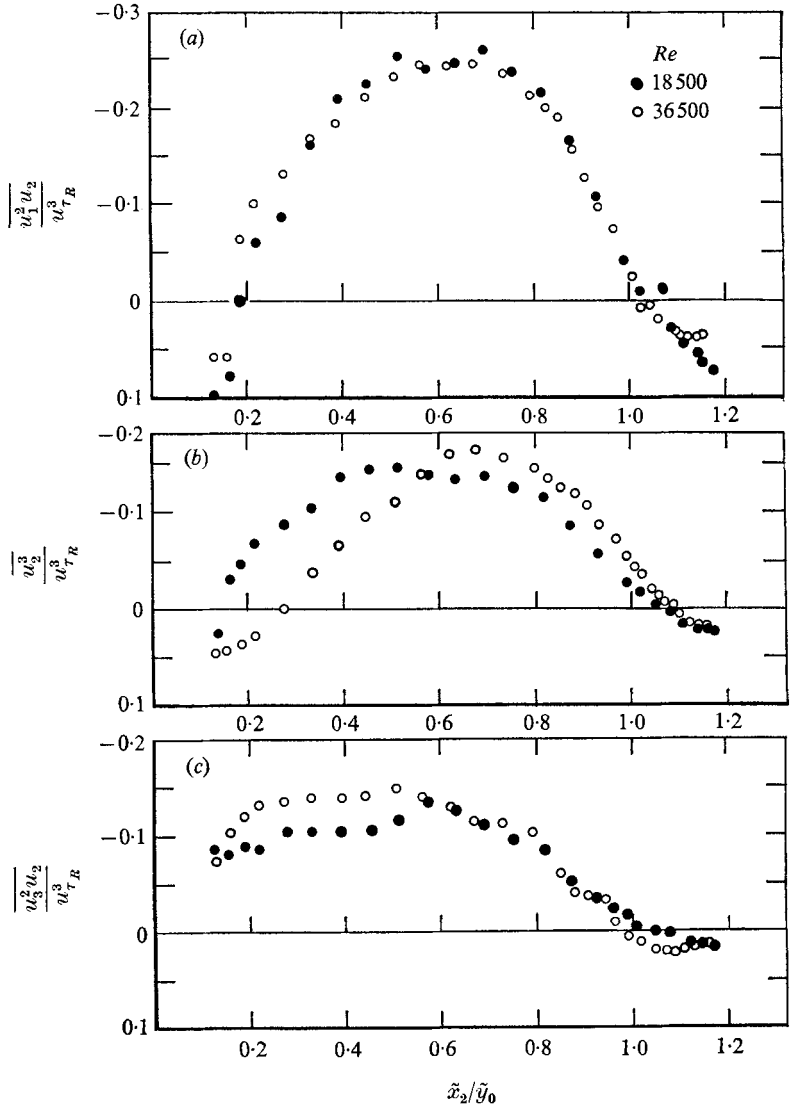

FIGURE 11. Profiles of turbulent triple correlations (components of turbulent energy diffusion).

The distribution of the skewness and flatness factors for the x_1 and x_2 components is shown in figure 14. The most striking feature of the skewness profiles is that for $0{\cdot}15 < x_2/D < 0{\cdot}8$, S_1 and S_2 vary in a closely parallel manner, with S_1 displaying somewhat higher (negative) values of skewness. This behaviour differs markedly from that measured by Comte-Bellot (1965) in a plane smooth channel. In her experiments, by virtue of the symmetric boundary conditions,

S_1 was symmetric about the mid-plane, attaining its largest magnitude at the centre-line; whereas S_2 was antisymmetric, falling to zero at the centre-line. (In her experiments, the centre-plane was of course the plane of zero shear stress.) In comparison, the present data show that the S_2 skewness factor falls to zero to the *left* (i.e. on the smooth-surface side) of the plane of zero shear stress whereas the magnitude of S_1 attains its maximum value to the *right* of y_0. This contrasting behaviour suggests that the S_1 and S_2 correlations may arise from eddies of rather dissimilar structure.

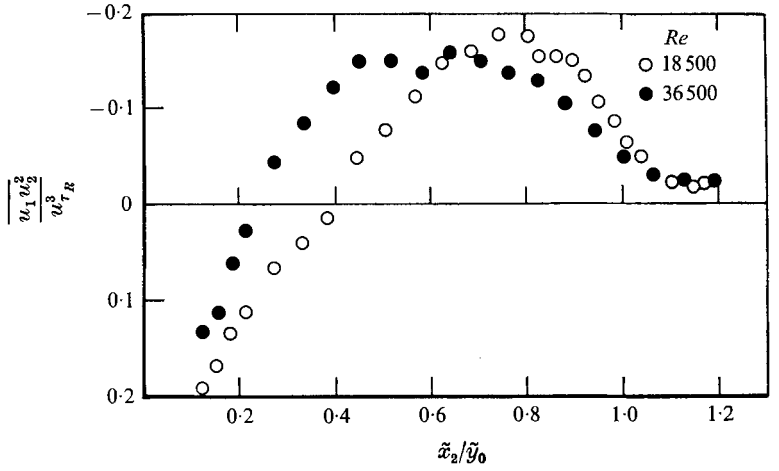

FIGURE 12. Turbulent diffusion of shear stress.

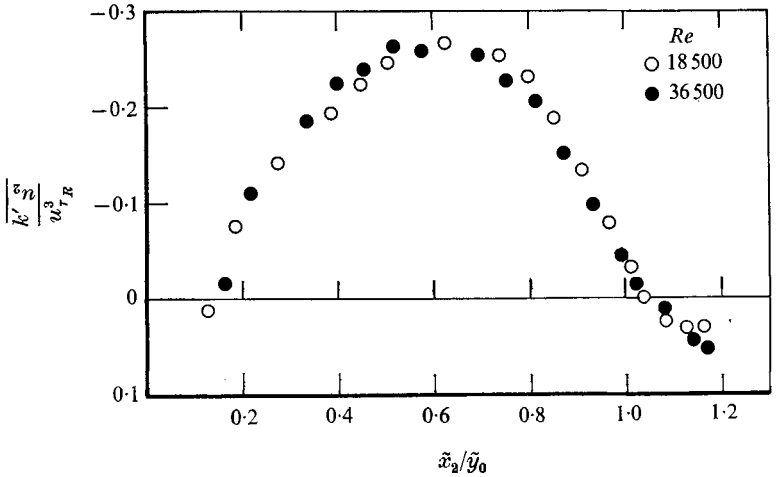

FIGURE 13. Turbulent diffusion of kinetic energy.

The u_1 and u_2 flatness factors exhibit substantially the same distributions across the channel. Over the half of the channel nearer the rough wall, the values for both components are, within the limits of experimental uncertainty, equal to 3·0, i.e. the value for a Gaussian distribution. A similar behaviour has been measured by Comte-Bellot (1965) in a smooth channel and by Lawn (1970) in a circular-sectioned pipe though their data exhibit somewhat larger values of F_2 than have been obtained here.

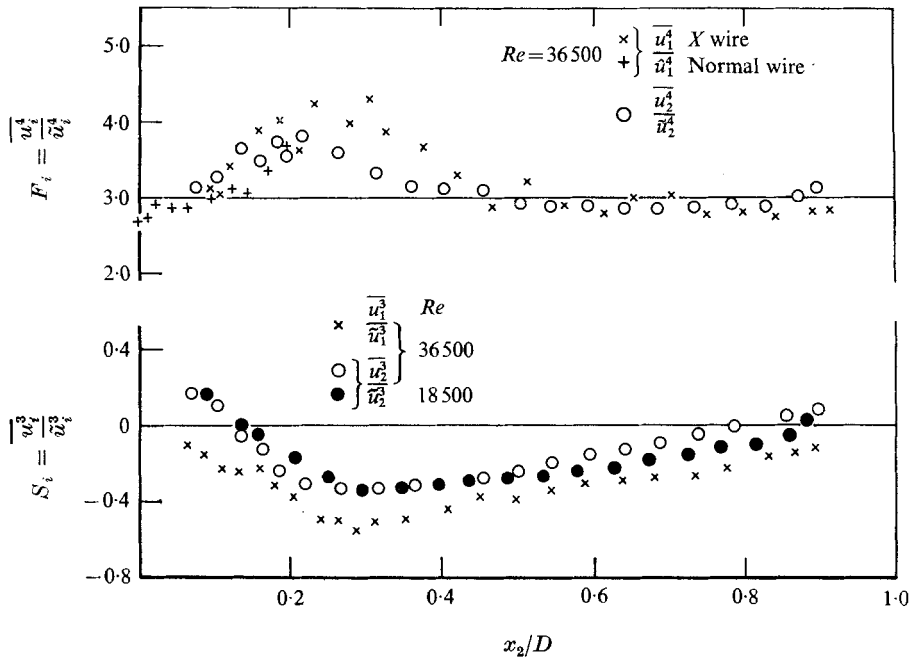

FIGURE 14. Flatness and skewness factors.

5. One-dimensional spectra

The spectral measurements were made at a single Reynolds number, $Re = 36\,500$, at a number of positions within the channel chosen to cover the flow regions of interest.

The spectra of $\overline{u_1^2}$ were measured in three ways: with a normal wire, and with cross-wires in the x_1, x_2 and x_1, x_3 planes. The resultant normalized profiles ϕ_{11} are shown in figure 15, wherein the abscissa has been successively offset by one decade for each position. The normalized spectral density ϕ_{ij} is defined as

$$\phi_{ij}(\kappa_1 D) \equiv F_{ij}(\kappa_1 D)/\overline{u_i u_j}, \tag{5.1}$$

where F_{ij} is the unnormalized spectra of $\overline{u_i u_j}$, so that

$$\int_0^\infty F_{ij}(\kappa_1 D)\, d(\kappa_1 D) = \overline{u_i u_j}.$$

The data obtained from the three sets of measurements are in close accord except at $x_2/D = 0{\cdot}5$, where the spectral profile measured with the normal wire exhibits rather lower values at high wave-numbers.

At the position closest to the smooth wall the spectra exhibit a κ_1^{-1} dependence over rather more than one decade, whereas for values of $x_2/D > 0{\cdot}2$ a $\kappa_1^{-\frac{5}{3}}$ variation is evident, again over rather more than a decade of the one-dimensional wave-number κ_1; these findings agree with those of measurements of Comte-Bellot (1965) and others. The corresponding normalized spectra ϕ_{22}, ϕ_{33} and ϕ_{12} are shown in figures 16–18. From these figures it is evident that the longitudinal

scale of the turbulence increases initially with distance from the smooth wall and reaches a maximum value near $x_2/D = 0{\cdot}5$. No appreciable region of these spectra exhibits a '$-\frac{5}{3}$' variation with wave-number; again, this result and the relative shape of the profiles are in agreement with spectra measurements in smooth channels and pipes (Comte-Bellot 1965, Lawn 1970). It is noted that figure 18 does not include a profile of the shear stress spectra near the plane of zero shear stress. The reason is that the shear stress in this region exhibits different signs in different regions of wave-number space; further discussion of this phenomenon is given below.

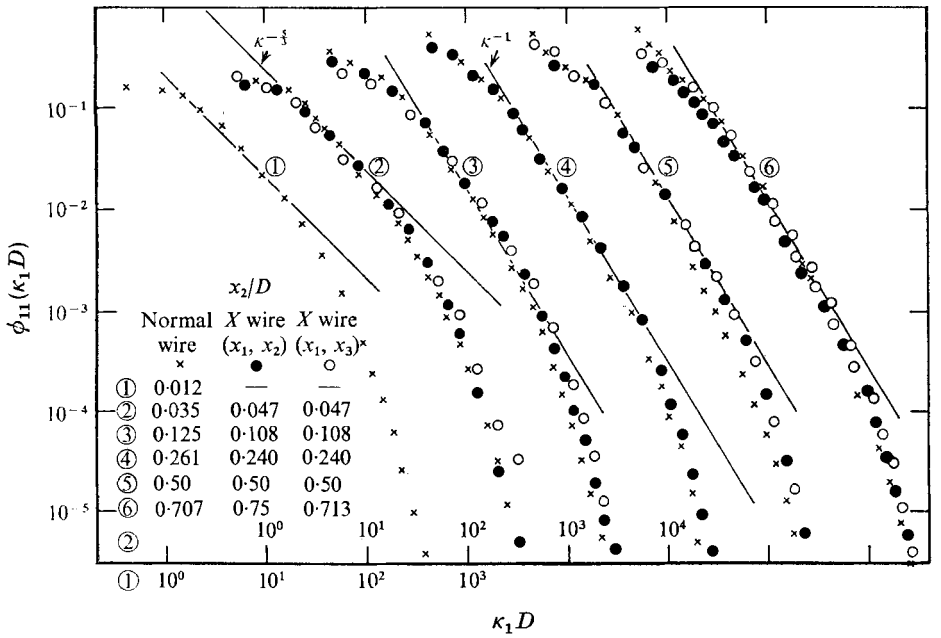

FIGURE 15. Normalized spectra of $\overline{u_1^2}$.

In order to provide comparison of the relative distributions with wave-number of the normal and shear stresses, the unnormalized spectral densities, $F_{ij}(\kappa_1)$, are plotted in figure 19 for positions near the smooth wall and at the mid-plane. The dashed line on the figure represents the variation of $F_{22}(\kappa_1)$ and $F_{33}(\kappa_1)$ which is implied by the isotropic relationship

$$F_{22}(\kappa_1) = F_{33}(\kappa_1) = \tfrac{1}{2}[F_{11}(\kappa_1) - \kappa_1 \partial F_{11}(\kappa_1)/\partial \kappa_1]. \tag{5.2}$$

At high wave-numbers, the measured spectra display close agreement with equation (5.2) particularly for the mid-channel position. As would be expected, the shear stress falls off more rapidly with wave-number than do the normal stresses. The value of F_{12} is still appreciable, however, where the F_{22} and F_{33} components follow closely the isotropic relation, equation (5.2).

The behaviour of the normal stress spectra at high wave-numbers may best be seen from figure 20, which plots all three components normalized with respect to the Kolmogorov length and velocity scales η and v, where $\eta \equiv \nu^{\frac{3}{4}} \epsilon^{-\frac{1}{4}}$, $v \equiv \nu^{\frac{1}{4}} \epsilon^{\frac{1}{4}}$, and ϵ is the dissipation rate of turbulence kinetic energy, evaluated from closure

of the turbulence energy equation. Although the experimental scatter is appreciable, considering the uncertainties in making high-frequency spectral measurements, the graphs display reasonably well a universal behaviour of the spectra at high wave-numbers. Figures 19 and 20 both suggest that, in many respects, the micro structure of the turbulence may be treated as isotropic.

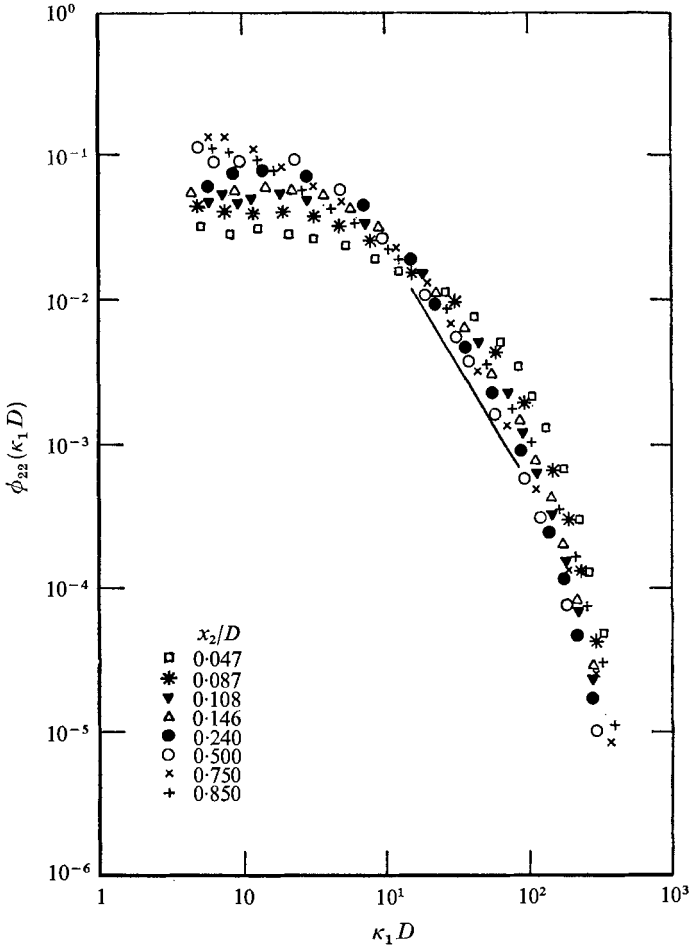

FIGURE 16. Normalized spectra of $\overline{u_2^2}$.

The one-dimensional spectrum of the shear correlation coefficient, defined as $R_{12}(\kappa_1) \equiv F_{12}(\kappa_1)/[F_{11}(\kappa_1)F_{22}(\kappa_1)]^{\frac{1}{2}}$, is plotted in figure 21 for various positions in the channel. A semi-logarithmic scale is adopted in order to show the actual sign of the correlation spectra. Over the portion of the channel closest to the rough wall the correlation coefficient displays a monotonic and rather rapid decay with increasing wave-number. (The measured increase of $R_{12}(\kappa_1)$ for $\kappa_1 D > 100$ is almost certainly a spurious result, in all probability attributable to instrument noise.†) The high values of the coefficient at low wave-numbers

† A referee has suggested that the measured behaviour could be caused either by the spatial separation of the wires or by the two spectrometers not being phase matched.

(greater than 0·8 for $x_2/D = 0{\cdot}85$) are indicative of a large well-organized eddy structure induced by the nearby ribbed surface. Over the half of the channel nearer the smooth surface the correlations are flatter with a maximum value not exceeding 0·5.

Of particular interest is the spectrum at $x_2/D = 0{\cdot}146$ close to the plane of zero shear stress. The shear correlation changes sign *twice* indicating that moderate wave-number eddies have a sign opposite to those of larger and smaller eddies. In view of this possibly surprising result, it is noted that the spectra at

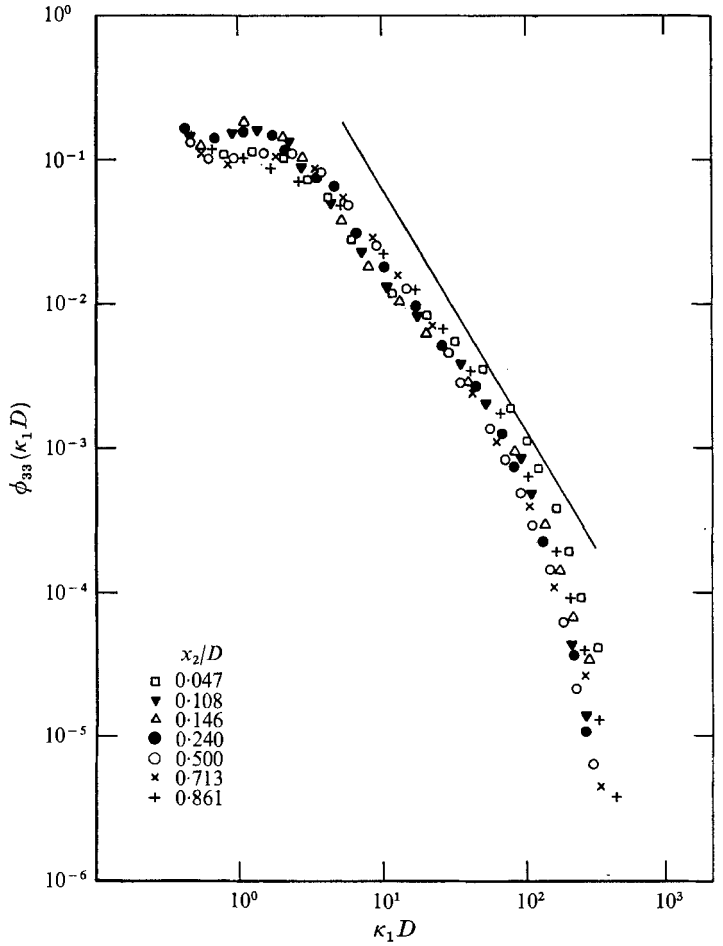

FIGURE 17. Normalized spectra of $\overline{u_3^2}$.

x_2/D equal to 0·108 and 0·087 (two sets of measurements are plotted for the latter position) each display a variation which is consistent with the measured profile at $x_2/D = 0{\cdot}146$; namely, a shift towards the sign of the correlation coefficient in the rough-wall region for values of $\kappa_1 D$ between 1·5 and 15. The phenomenon appears to be caused by a substantial migration of eddies within the above band of wave-numbers from their origin in the rough-wall region to the vicinity of the smooth wall.

Measurements of the shear correlation coefficient in homogeneous shear flow (Champagne *et al.* 1970) and in pipe flow (Lawn 1970) display no such change of sign. The behaviour measured in the present channel may thus be attributed to the strongly asymmetric boundary conditions of the flow. Finally, it is recorded that at $x_2/D = 0{\cdot}047$ ($x_2^+ \approx 50$) the correlation spectrum appears to be quite unaffected by the structure of the flow in the rough-wall region.

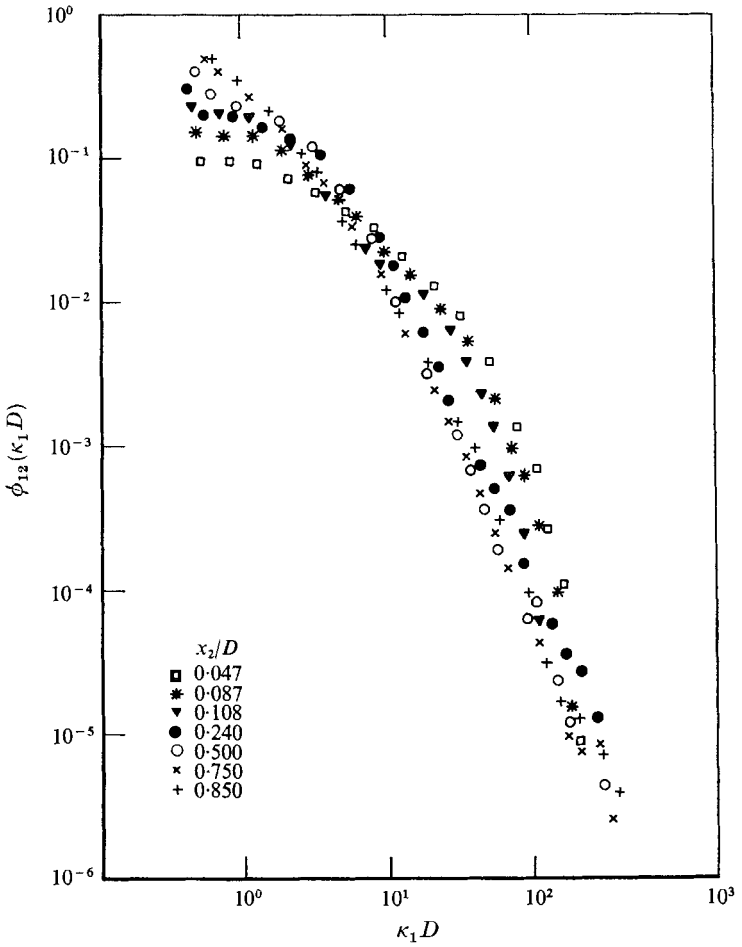

FIGURE 18. Normalized spectra of turbulent shear stress.

Figure 22 presents one-point spectra of the triple correlations of the velocities u_1 and u_2 measured at three positions in the channel. The data are presented in the form of normalized spectral densities

$$\phi_{ij,l}(\kappa_1 D) \equiv \frac{\overline{u_i u_j(\kappa_1 D)\, u_l(\kappa_1 D)}}{\overline{u_i u_j u_l}}, \tag{5.3}$$

where i, j and l take values 1 or 2 in five different permutations. The spectra $\phi_{12,1}$ and $\phi_{22,2}$ are two of the three components of the general term $\phi_{i2,i}$ the divergence of which represents the spectral density of the net turbulent diffusion

of kinetic energy in direction x_2. This spectral form, it is noted, provides information about the energy diffusion of eddies of the considered wave-number. The alternative spectral grouping, $\phi_{ii,2}$, may be shown to represent the spectral diffusion of $\overline{u_i^2}$ for which eddies of wave-number κ_1 *are responsible* (Bradshaw & Ferriss 1965). Correspondingly, $\phi_{12,2}$ represents the diffusion of shear stress by eddies of the considered wave-number whereas the shear-stress diffusion of eddies of wave-number κ_1 is given by $\frac{1}{2}(\phi_{12,2}+\phi_{22,1})$. In figure 22, the latter grouping which involves the arithmetic mean of two ϕ's is shown by a broken line.

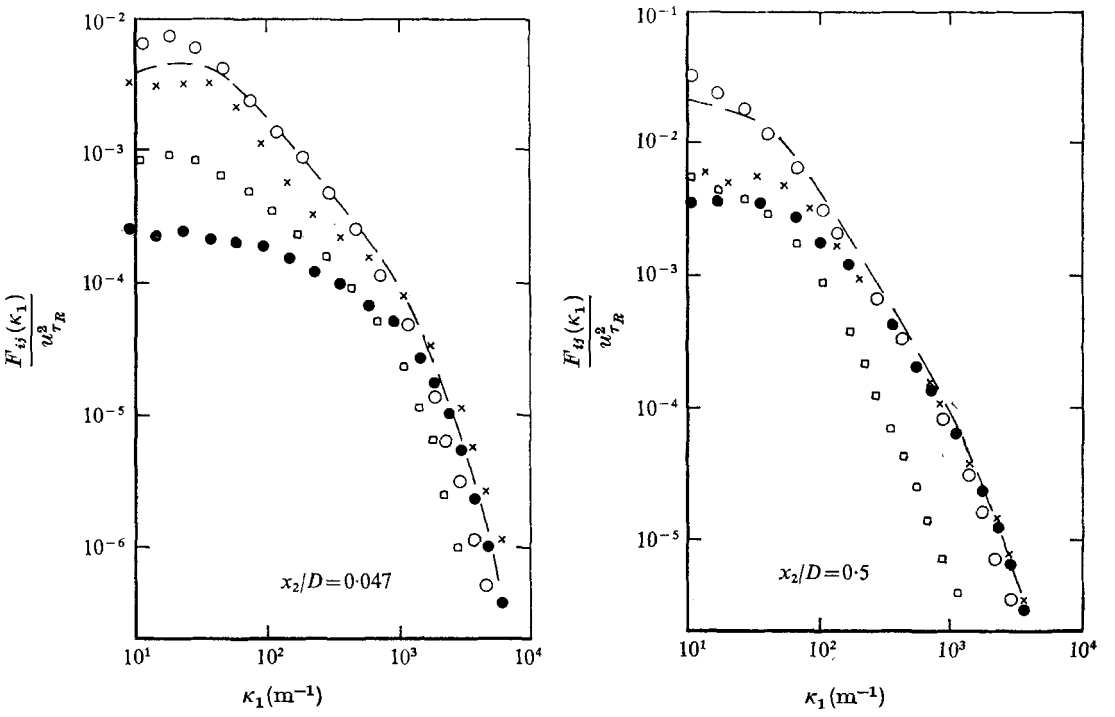

FIGURE 19. Comparison of unnormalized power spectra. ○, F_{11}; ●, F_{22}; ×, F_{33}; □, F_{12}.

At $x_2/D = 0{\cdot}047$, the position closest to the smooth wall, there is no significant distinction between the various spectral forms. Further from the wall, however, a difference emerges which appears worthy of comment: namely, that the spectra are grouped into two pairs $\phi_{ij,1}$ and $\phi_{ij,2}$. The spectral density of the former pair falls off at considerably lower wave-numbers than the latter. The difference in shape between these two pairs of spectra is qualitatively similar to the difference between the ϕ_{11} and ϕ_{22} spectra of kinetic energy (figures 15 and 16), suggesting that the turbulent diffusion velocities of a particular wave-number, $u_1(\kappa_1)$ and $u_2(\kappa_1)$, exert a dominating effect upon the shape of diffusion spectra of the triple correlations. A consequence of this pairing is that eddies responsible for the diffusion of shear stress (the $\phi_{12,2}$ spectrum) are of a predominantly higher wave-number than the shear stress bearing eddies which are diffused (the spectrum of $\frac{1}{2}(\phi_{12,2}+\phi_{22,1})$ denoted by the broken line).

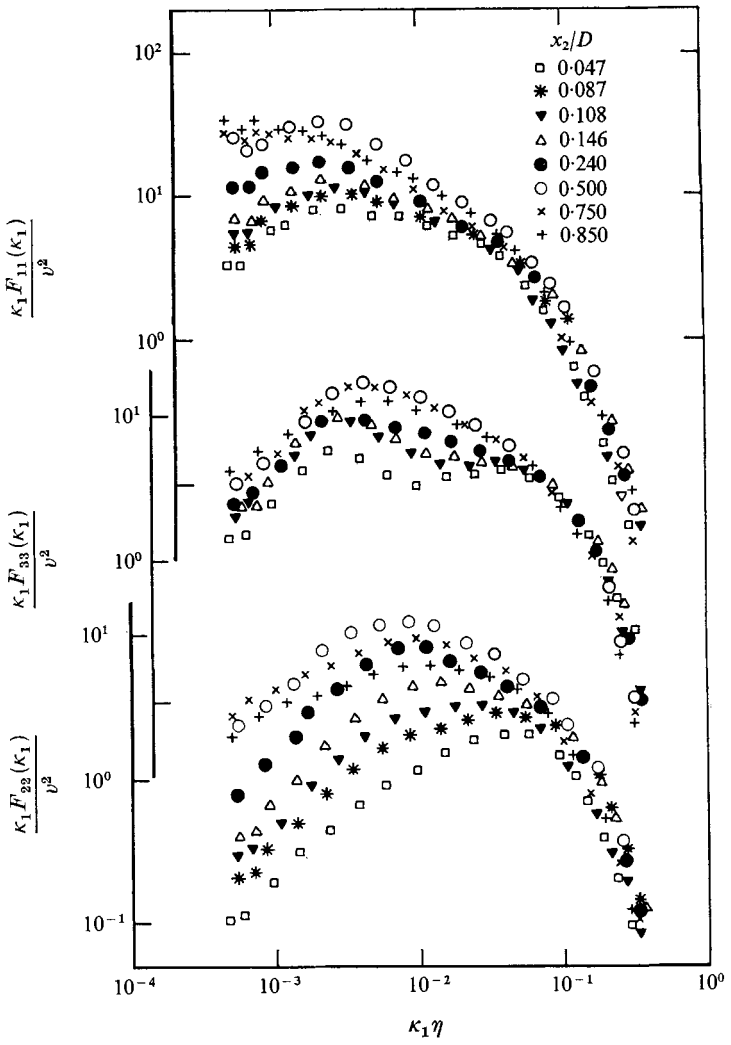

FIGURE 20. Spectra of normal stress components normalized with Kolmogorov scales.

6. Length scales of the turbulent motion

At a single Reynolds number, $Re = 36500$, measurements were made of the two-point lateral correlation coefficient of the u_1 velocity component, defined as

$$R_{11}(0,r_2,0) \equiv \frac{\overline{u_1(x_2)\,u_1(x_2+r_2)}}{\overline{u}_1(x_2)\,\overline{u}_1(x_2+r_2)}. \tag{6.1}$$

The measurements were obtained by means of two gold-plated hot wires aligned normal to the flow, one of which could be moved relative to the other in the x_2 direction. Measurements of the correlation coefficient were made at a dozen positions across the channel but for clarity only data for half of these are presented in figure 23.† Measurements at $x_2/D = 0{\cdot}42$ were made on two separate occasions and, as figure 23 shows, the two sets of data exhibit satisfactory consistency.

† More extensive data are provided by Hanjalić (1970).

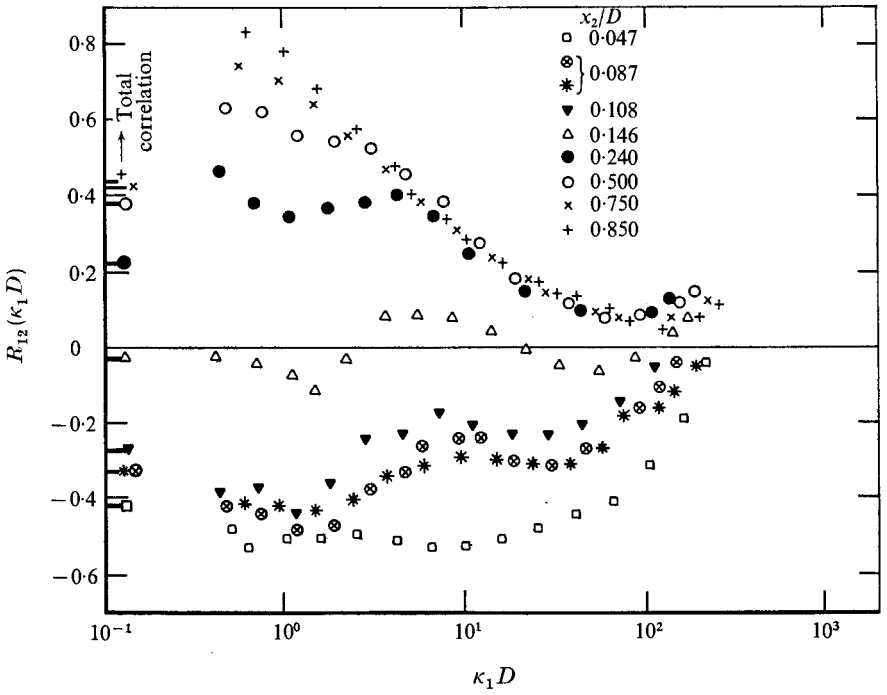

FIGURE 21. Spectra of shear correlation coefficient.

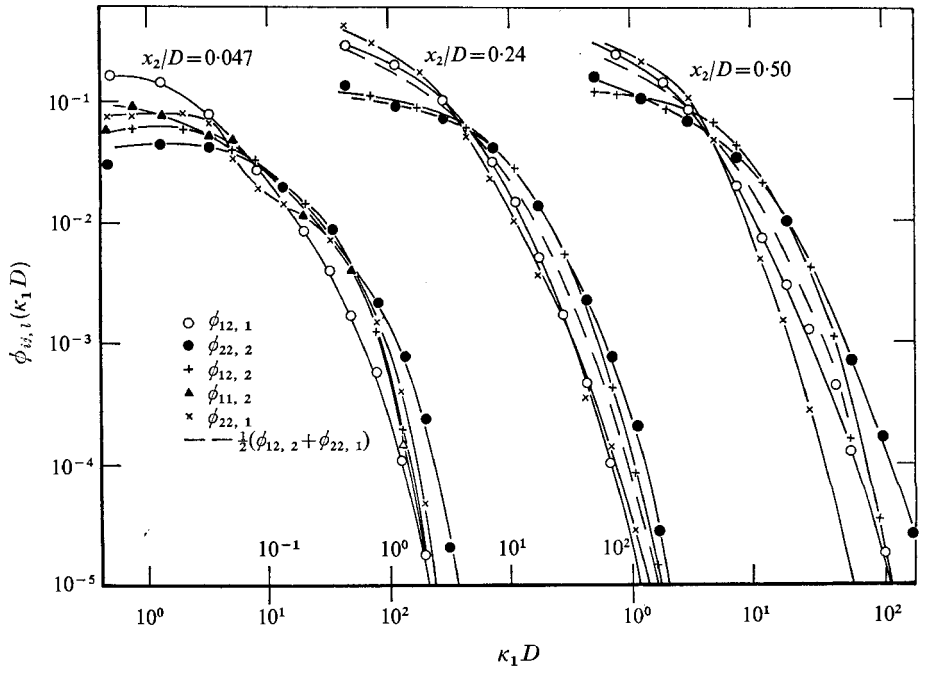

FIGURE 22. Normalized spectra of the triple velocity correlations.

It is noted first that the space correlations for the three central positions in the channel are appreciably asymmetric, an expected result in view of the strong lateral inhomogeneity of the flow. Moreover, it is seen that the correlation coefficient becomes negative at sufficiently large values of r_2. Perhaps the most interesting feature to emerge is that for values of x_2/D between 0·2 and 0·5 the correlation decreases linearly or with small convex curvature with increasing separation between the wires. This finding, which is in marked contrast to the concave curvature displayed in a smooth channel (Comte-Bellot 1965), is indicative of a pattern of eddies of rather uniform size.† Closer to the smooth wall, the correlation coefficients exhibit a behaviour similar to those measured in a smooth channel; in this region, turbulence generated by the influence of the rough wall is suppressed by the structure originated at the smooth wall.

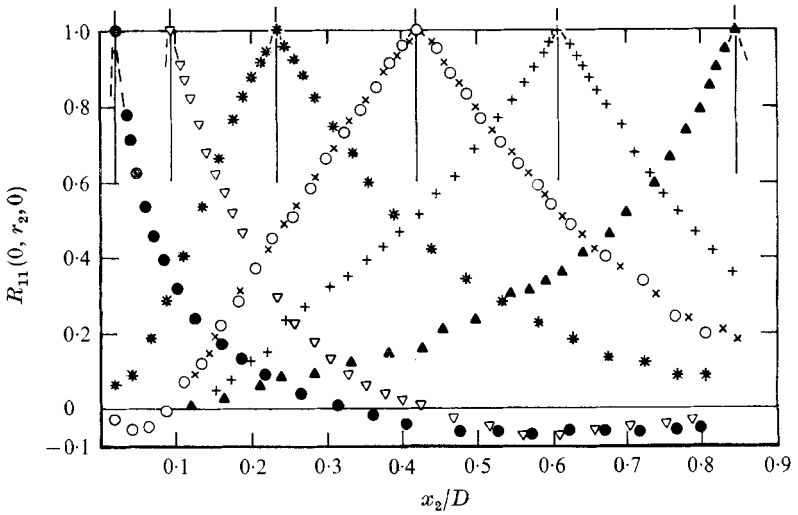

FIGURE 23. Lateral space correlation coefficient, $R_{11}(0, r_2, 0)$.

Figure 24 shows the profile of lateral integral scale, L_{211}, obtained by integration of $R_{11}(0, r_2, 0)$:

$$L_{211} = \int_{-\infty}^{\infty} R_{11}(0, r_2, 0)\, dr_2. \tag{6.2}$$

Unlike the profiles of turbulent and mean flow velocities L_{211} is nearly symmetric. The overall shape is not unlike those in symmetric ducts though the peak level attained is appreciably higher than in a plane symmetric channel. The result provides further evidence that $\tilde{y}_0$ (the distance from the rough wall to the plane of zero shear stress) rather than $\frac{1}{2}D$ may be taken as the effective half-width of the channel wall.

Estimates of the *longitudinal* integral scales, shown in figure 25, were made from the low wave-number asymptote of $F_{ij}(\kappa_1)$ by means of the Fourier transformation

$$L_{1ij} = \int_0^{\infty} R_{ij}(r_1, 0, 0)\, dr_1 = \frac{\pi}{2\overline{u_i u_j}} \lim_{\kappa_1 \to 0} F_{ij}(\kappa_1).$$

† See Townsend (1956, p. 15).

The difficulty of measuring the spectra at very low wave-numbers and the uncertainty of the applicability of Taylor's hypothesis conspire to place the absolute accuracy of these data in doubt. Any errors may, however, be expected to be systematic and the curves may be taken to indicate the relative levels of the length scales.

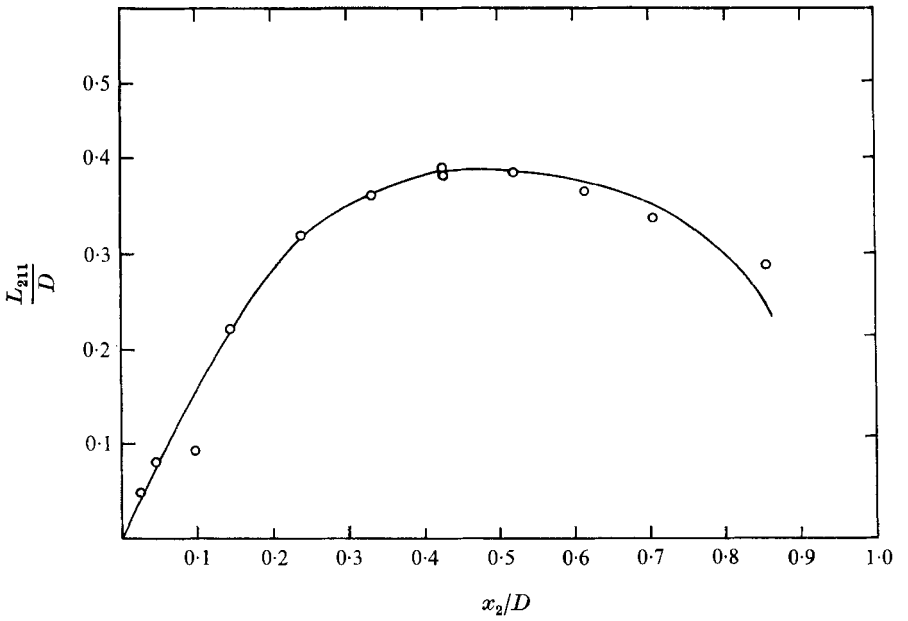

FIGURE 24. Profile of lateral integral scale, L_{211}.

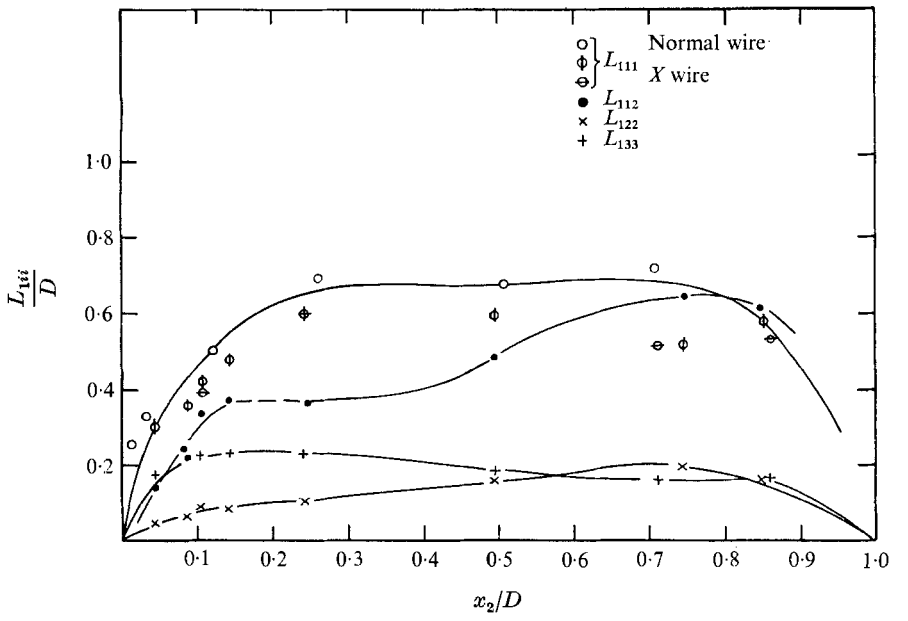

FIGURE 25. Profiles of longitudinal integral scales.

Like the lateral integral scale, the profile of L_{111} appears to be virtually symmetric, its shape being similar to, but with a level about twice that of, L_{211}. The scales L_{122} and L_{133} are much smaller (in agreement with Comte-Bellot's symmetric-channel data). The former is appreciably skewed towards the rough wall whereas, in contrast, L_{133} attains its maximum value close to the plane of zero shear stress. Finally, L_{112} is strongly asymmetric, similar in shape to L_{122}. As the plane of zero shear stress is approached, the value of this length scale will probably approach $\pm\infty$ because the zero-wave-number asymptote is unlikely to vanish where the total correlation is zero (cf. figure 21); for this reason the line joining the data in the vicinity of y_0 has been marked with a broken line.

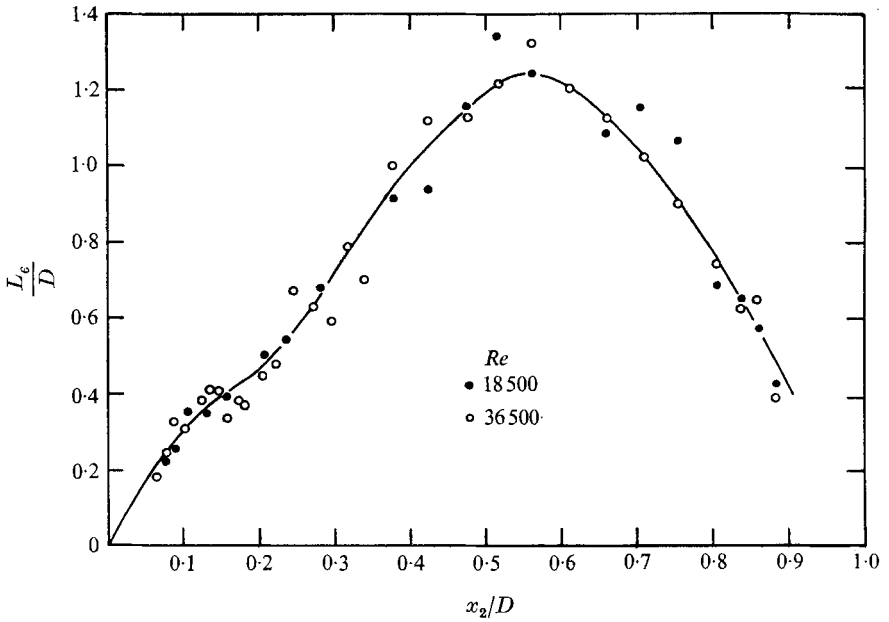

FIGURE 26. Profile of dissipation length scale.

The profile of the scalar dissipation length scale $L_\epsilon = k^{\frac{3}{2}}/\epsilon$, is shown in figure 26, wherein k denotes the turbulence kinetic energy and the dissipation rate has been obtained as the closing term in the energy-balance equation (§7). There is a certain amount of scatter in the data but the profiles for the two Reynolds numbers show reasonable agreement; both, it is noted, exhibit a point of inflexion near $x_2/D = 0{\cdot}2$. In pipe flow, L_ϵ reaches its maximum value at about mid-radius and diminishes towards the centre-line. Figure 27 indicates that, near the two walls, the dissipation length scale follows a similar behaviour in both the rough- and smooth-wall regions. Where these dissimilar wall structures interact, the distribution of L_ϵ adjusts to match the scales in the two regions thus leading to the inflexion point.

The longitudinal components of the Taylor microscale, λ_{1ii}, are presented in figure 28. The data were evaluated from the second moment of the energy spectra

$$\lambda_{1ii} = \left[\int_0^\infty \kappa_1^2 \phi_{ii}(\kappa_1)\, d\kappa_1\right]^{-\frac{1}{2}}. \tag{6.3}$$

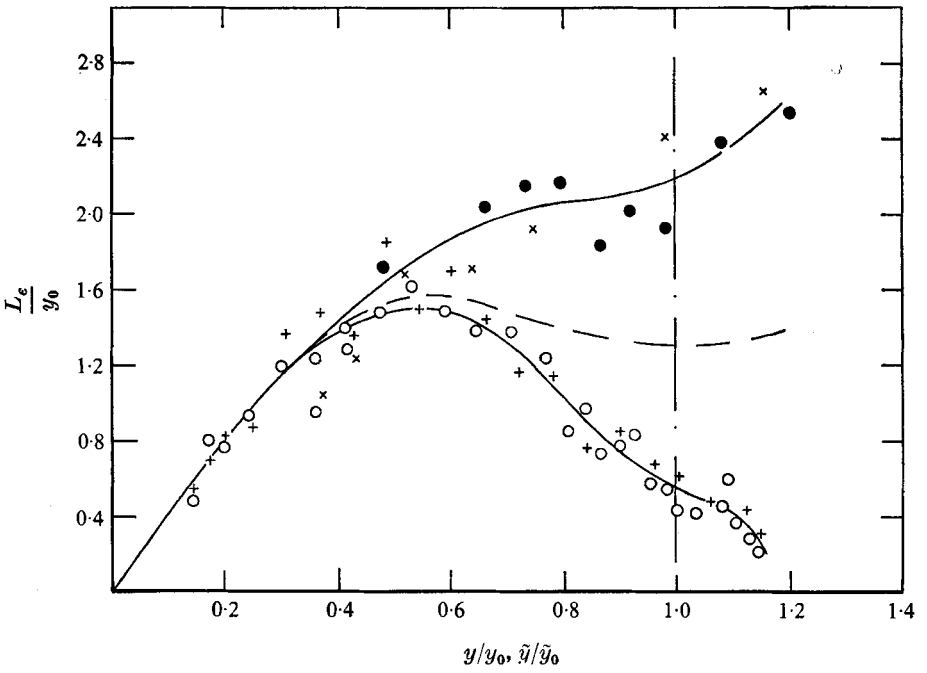

FIGURE 27. Distribution of dissipation length scales in smooth- and rough-wall regions.

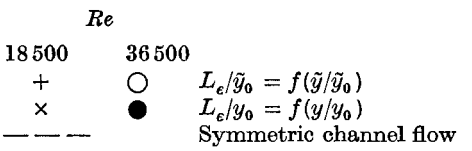

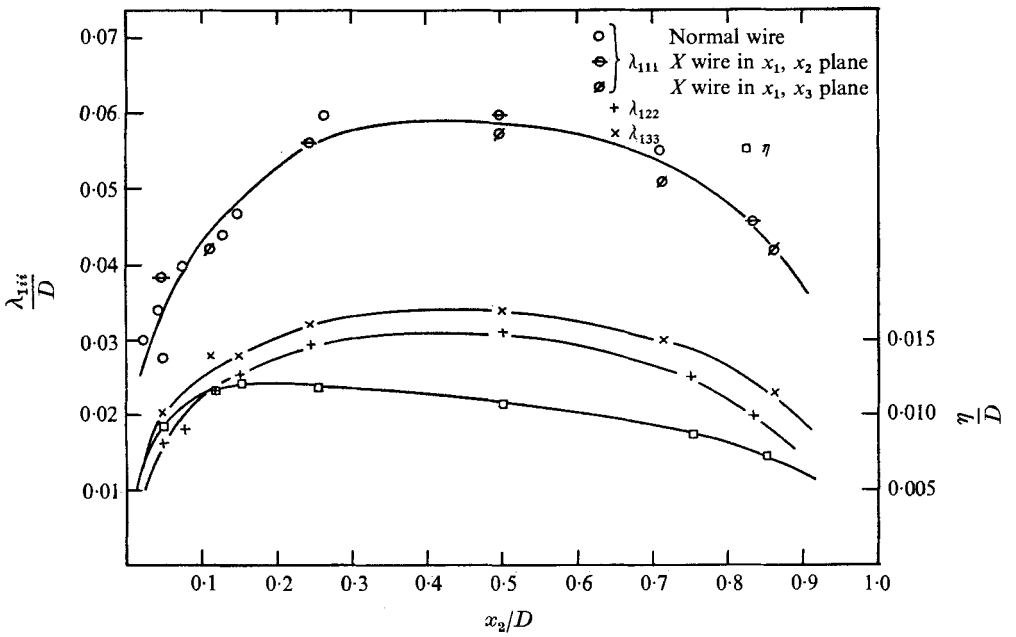

FIGURE 28. Distribution of Taylor and Kolmogorov microscales.

The scales are approximately symmetric with respect to the mid-plane of the channel though λ_{111} is appreciably larger than is implied by the isotropic relationship

$$\lambda_{111} = \lambda_{122}\sqrt{2} = \lambda_{133}\sqrt{2}. \tag{6.4}$$

Perhaps, as a referee has suggested, this discrepancy is attributable to the finite-wire-length effects for which Wyngaard's (1968) correction attempts to compensate.

For comparison, the Kolmogorov microscale η, representative of the size of the dissipative eddies, is also shown in figure 28, the ordinate being enlarged by a factor of two for clarity. The figure shows that the maximum value of η is only about one-sixth that of λ_{111}, indicating that the Taylor microscale does not provide a very precise indication of the scale of the dissipative motions.

7. Energy balance

For fully developed plane-channel flow the equation for the conservation of turbulent kinetic energy may be written

$$-\overline{u_1 u_2}\frac{dU_1}{dx_2} - \frac{d}{dx_2}\left(\overline{k' u_2} + \frac{\overline{p u_2}}{\rho}\right) - \epsilon = 0, \tag{7.1}$$

where p refers to the instantaneous value of pressure fluctuations. The equation expresses the fact that the energy supply to turbulence from the mean motion by the action of shear stress (the generation term) and by turbulent diffusion (owing to the velocity and pressure fluctuations) is equal to the rate at which the turbulent motion dissipates the energy.

In the present experiments the generation term and the velocity-diffusion term have been measured directly. The measurement of the pressure-diffusion term, which poses severe experimental difficulties (which, to the authors' knowledge, have not yet been overcome) was not attempted. There is some evidence to suggest, however, that it may be negligibly small except in the immediate vicinity of a wall. With this term neglected, therefore, equation (7.1) has been employed to determine the dissipation rate as the closing term. The resultant energy balance is displayed in figure 29. The figure shows that near both walls the diffusion term is far outweighed by the generation and dissipation terms. In the neighbourhood of the plane of zero shear stress, however, it is the large diffusional influx of energy which makes good the loss by dissipation and by the 'generation' term becoming negative.

While the magnitude of this energy transfer from the turbulent to the mean motion is not significant compared with those of the diffusion and dissipation terms, the phenomenon itself is perhaps of sufficient interest to merit further scrutiny. It is clear from the profile of the shear stress spectra at $x_2/D = 0{\cdot}146$ (figure 21) that it is the moderate wave-number motions, $1{\cdot}5 < \kappa_1 D < 15$, with which the negative generation is mainly associated. Moreover, from figure 22, it emerges that much of the diffusion of energy and shear stress is likewise associated with the same range of wave-numbers. The following thus seems to be a consistent description of the processes which conspire to produce a

region of negative energy generation. In the vicinity of each wall is established a flow structure characteristic of the nearby surface. In the region where these two dissimilar flow structures interact, there is a substantial diffusive transport of energy and shear stress from the rough- to the smooth-wall region. The diffused shear stress bears a sign opposite from that locally produced and over a limited region the total 'generation' is consequently negative.

To provide some independent check on the values of the dissipation term estimated above, the term was also evaluated from the $\overline{u_1^2}$ energy spectra by the

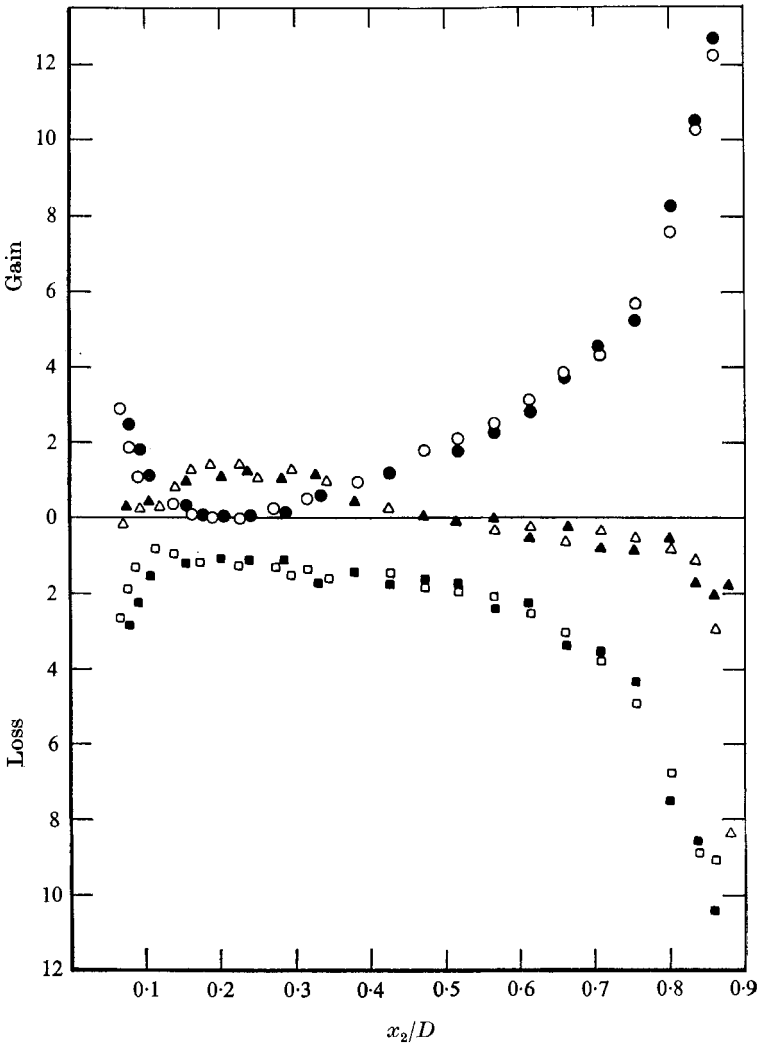

FIGURE 29. Turbulent kinetic energy balance.

	Re 18 500	36 500
$-(\overline{u_1 u_2} dU_1/dx_2) D/u_{\tau_R}^3$	●	○
$-(d\overline{k' u_2}/dx_2) D/u_{\tau_R}^3$	▲	△
$\epsilon D/u_{\tau_R}^3$	■	□

method proposed by Bradshaw (1969). A tangent with $-\frac{5}{3}$ slope was fitted and the dissipation was then calculated from the relation

$$\epsilon = [F_{11}(\kappa_1)\kappa_1^{\frac{5}{3}}/0{\cdot}51]^{\frac{3}{2}}. \tag{7.2}$$

In figure 30 the results are compared with the values of ϵ estimated from the energy equation above. A deviation between the two estimates of about 20% appears at $x_2/D = 0{\cdot}5$ but in other regions of the channel the agreement is satisfactory.

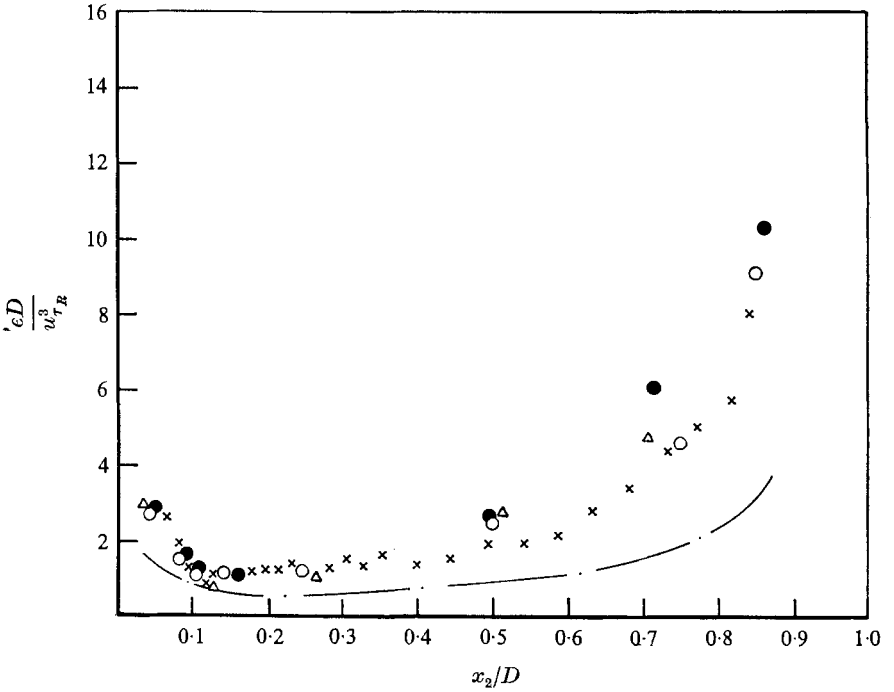

FIGURE 30. Estimates of turbulence energy dissipation rate.

× By difference from equation (7·1).
△ Normal wire.
○ X-wire in x_1, x_2 plane
● X-wire in x_1, x_3 plane
$\epsilon = \left(\frac{F_{11}(\kappa_1)\kappa_1^{\frac{5}{3}}}{0{\cdot}51}\right)^{\frac{3}{2}}$
—·— From Taylor microscales.

A third estimate of dissipation was obtained by calculating three of the nine dissipative terms through the Taylor microscale, λ_{1ii}. The chain line on figure 30 represents the dissipation calculated from the isotropic relationship

$$\epsilon = 3\nu\left[\left(\frac{\tilde{u}_1}{\lambda_{111}}\right)^2 + \left(\frac{\tilde{u}_2}{\lambda_{122}}\right)^2 + \left(\frac{\tilde{u}_3}{\lambda_{133}}\right)^2\right]. \tag{7.3}$$

Although the resultant profile of dissipation exhibits a similar shape to that obtained by closure of the turbulence energy equation, the magnitude of the former is only about one half that of the latter. The result suggests that the dissipative motions do not possess in all respects the character of isotropic turbulence. This finding is consistent with the measurements of Klebanoff (1955) and Laufer (1954).

8. Summarizing remarks

The discussion in the preceding sections has examined in turn various properties of the mean and turbulent flow in an asymmetric plane channel. In conclusion it may be helpful to consider the structure which collectively emerges from the data of the three flow regimes in the channel.

First, in the rough-wall region, extending from the rough surface to approximately the mid-plane of the channel, the flow structure appears to be determined solely by the nature of the rough-wall boundary conditions. This conclusion is supported by the universal character of the mean velocity profiles (figure 5) and by the uniform value of the shear correlation coefficient (figure 9). None of the profiles in this region exhibited detectable influences of Reynolds number. Within about three rib heights of the surface the turbulence structure showed signs of being affected by the discrete roughness elements: the shear correlation coefficient exhibited values as high as 0·8 at low wave-number and the turbulent diffusive flux of energy (neglecting pressure diffusion) was up the energy gradient. Both these results suggest the presence of a better co-ordinated eddy structure than is present near a smooth wall.

The present investigation and the earlier study by the authors provide a variety of data which support the conclusion that near the smooth surface, too, there is likewise a region of local equilibrium where neither the mean nor the turbulent structure of the flow appears affected by the adjacent rough-wall structure. The result is perhaps chiefly of interest because of the questions it raises concerning the flow in a smooth channel. For example, we have found that the mean velocity profile for $x_2^+ < 150$ is the same irrespective of whether the roughened opposite wall of the channel is 28 mm or 54 mm away; and that the measured profiles accord with Patel's (1965) proposal for external boundary layers. Yet, the profiles are appreciably different from the measurements of Comte-Bellot (1965) in a smooth channel and even more substantially different from those of Clark (1968) (figure 4). It is probably significant that the data of $\tilde{u}_1$ normalized with the smooth-wall friction velocity (see appendix) should show the same relative discrepancies among the three investigations (i.e. Clark's is the highest, Comte Bellot's the next and the present author's data the lowest of the three, but in good agreement with the data of Van Thinh (1967)). This result suggests that errors in the determination of the smooth-wall shear stress may be a major cause of the variations among the data.

The region where the smooth- and the rough-wall structures interact is where the chief emphasis of the present investigation has been placed. Evidence of this interaction is provided by the profiles of mean velocity, turbulent stresses and triple correlations. Typically, in the 54 mm channel, the mean velocity gradient vanished at $1{\cdot}25y_0$, whereas the turbulence energy reached its minimum at about $0{\cdot}75y_0$, which was also the location at which the diffusion of turbulence energy became zero. In the energy-balance equation, this region was distinguished by the high net diffusional flux of energy from the rough-wall region. The diffused eddies bear a shear stress of opposite sign from those originating near the smooth wall, however, and over most of the region their

interaction with the mean flow tends to diminish the prevailing level of turbulence energy.

Apart from the double sign reversal in the spectrum of shear stress, near y_0, the spectral profiles of the shear and normal stresses were not appreciably dissimilar from those measured in the central region of a plane channel. In particular, Bradshaw's proposal for determining the energy dissipation rate from the inertial subrange of the $F_{\overline{u^2}}(\kappa)$ spectrum gave values of ϵ which were generally consistent with those found from the energy-balance equation with pressure-diffusion terms neglected. Moreover, despite the strong overall anisotropy of the flow, there was much evidence to suggest that the dissipative motions were isotropic.

In general, both the macro- and microturbulent length scales exhibit much less asymmetry with respect to the mid-plane than do the turbulence velocity correlations. The lateral integral scale L_{211}, however, attains an appreciably larger proportion of the channel width than in a smooth channel. Thus, $\tilde{y}_0$, the width of the rough-wall originated flow, appears to determine the lateral dimensions of the largest-scale motions. By comparison, the longitudinal integral scales are comparable in magnitude to those in a smooth channel or in a pipe.

The research reported here has been sponsored by the Berkeley Nuclear Laboratories of the CEGB. We wish to acknowledge both this financial support and the sustained interest in the research by the Board's staff. Our colleagues at Imperial College, Mr P. Bradshaw and Dr J. H. Whitelaw, have substantially aided the research through discussions and through the loan of many electronic instruments.

Appendix. The streamwise turbulence intensity near a smooth wall

The profile of streamwise turbulence intensity in the immediate neighbourhood of a smooth wall has been the subject of a number of experimental studies. Here we limit attention to flows in a plane channel and provide comparison between our own data in a rough–smooth channel with those of other workers in a symmetric configuration.

The profiles of u_1/u_{τ_s} are shown in figure 31 as a function of x_2^+. The first impression to emerge is that of the very large variation among the measurements; for example, the peak value of u_1/u_{τ_s} in Clark's channel is some 80 % higher than Laufer's (1951) in his 25 mm channel. Let us, however, look for consistencies among the smooth-channel data and the present measurements before considering the differences. All the profiles display similar shapes with the maximum intensity occurring at a value of x_2^+ of between 15 and 20; this is within the range indicated by measurements in pipe flow (Laufer 1954; Coantic 1967) and in external wall boundary layers (Klebanoff 1955). Moreover, focusing attention now on Comte-Bellot's and the authors' (1968) data, a consistent effect of Reynolds number is displayed. As the Reynolds number is increased, in a particular channel, the peak value of $\tilde{u}_1/u_{\tau_s}$ decreases. The decay with x_2^+ is more gradual however and consequently for $x_2^+ > 70$ the normalized turbulence intensity increases slowly with Reynolds number.

The major discrepancy among the considered data is the *magnitude* of the turbulence intensities in each investigation. The early data of Laufer had suggested that the width of the channel itself might affect the peak level of turbulence intensity. However, the more recent data of Van Thinh (1967), Comte-Bellot (1965) and Clark (1968), which were obtained in channels of almost the *same* dimensions, also display considerable variation in the maximum value of $\tilde{u}_1/u_{\tau_s}$ (2·3, 2·8 and 3·2 respectively for approximately the same Reynolds numbers).

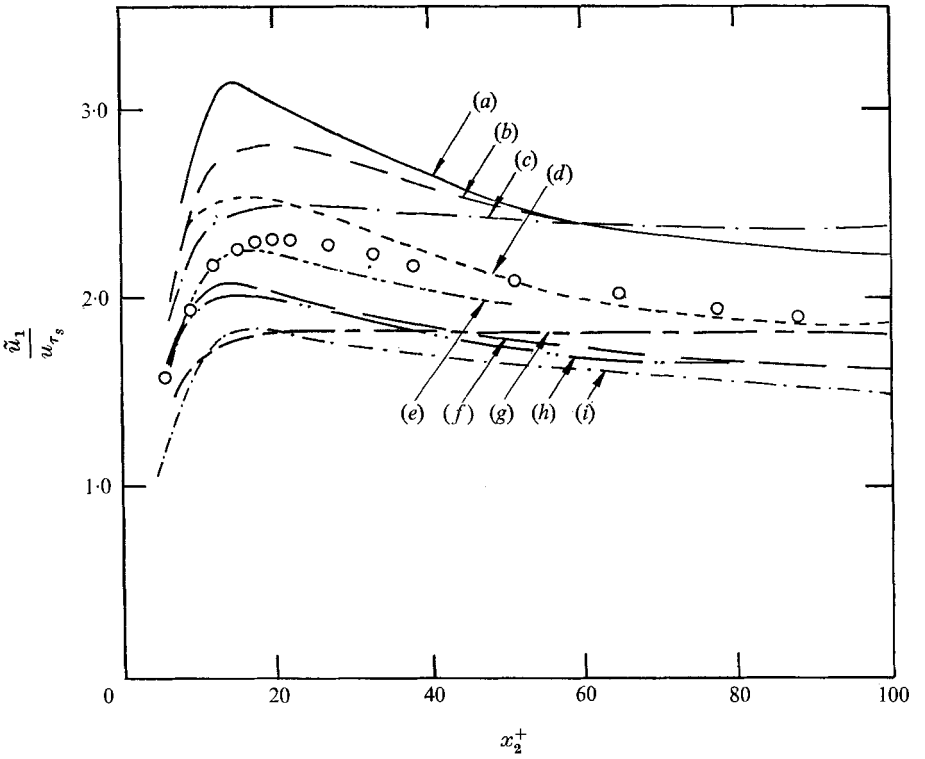

FIGURE 31. Longitudinal turbulence intensity near smooth wall. Clark (1968): (*a*) Re = 45600; Comte-Bellot (1965): (*b*) Re = 57000, (*c*) Re = 123000; Laufer (1951), 125 mm channel: (*d*) Re = 30800; Van Thinh (1967): (*e*) Re = 40000; Hanjalić & Launder (1968): (*f*) Re = 18500; (*g*) Re = 55200; (*h*) Re = 10200 (28 mm channel); Laufer (1951), 25 mm channel: (*i*) Re = 12000. ○, present data; Re = 36000.

The authors' earlier data (Hanjalić & Launder 1968) in the smooth–rough channel exhibit maximum values of $\tilde{u}_1/u_{\tau_s}$ of between 1·8 and 2·1 according to Reynolds number. It might at first be supposed that here the presence of discrete ribs on the opposite surface (providing a strong source of pressure fluctuations) could lead to the generation of 'inactive' motions which would cause the $\tilde{u}_1$ profiles to differ from those in a smooth channel – even in the immediate vicinity of the surface. However, the difference between the measured intensity profiles in the 28 mm and 54 mm channels is not large even though the ratio of rib height: channel width was almost twice as large in the smaller duct than in the larger. It thus seems likely that the structure within the region shown in

figure 31 is sensibly unaffected by the texture (and the distance removed) of the opposite surface.

In the present investigation, the near-wall region was re-examined at only one Reynolds number (though two profiles were taken on different occasions, these two sets of data were indistinguishably different). The instrumentation for the present tests differed from the earlier work in that a transistorized anemometer and linearizer were employed and gold-plated boundary-layer probes used for the traverses; it may be expected that these changes improved the reliability of the data. It is seen from the figure that the resultant $\tilde{u}_1$ profile displays appreciably higher values than the earlier measurements, being in close agreement with Van Thinh's and Laufer's (125 mm channel) data. Of course, the agreement with these workers' measurements is not a conclusive proof of their mutual accuracy. In view of the very sophisticated sampling technique adopted by Van Thinh, however, it appears likely that, at a channel Reynolds number of about 40000, the peak value of $\tilde{u}_1/u_{\tau_s}$ does lie between about 2·3 and 2·5.

REFERENCES

Beguier, M. C. 1965 Mesures des tensions de Reynolds dans un écoulement dissymétrique en régime turbulent incompressible. *J. Mécanique*, **4**, 320–334.

Bradshaw, P. 1969 Conditions for the existence of an inertial subrange in turbulent flow. *N.P.L. Aero. Rep.* 1220 (ARC 28664).

Bradshaw, P. & Ferriss, D. H. 1965 The spectral energy balance in a turbulent mixing layer. *N.P.L. Aero Rep.* 1144–*Aero. Res. Counc.* 26743.

Champagne, F. H., Harris, V. G. & Corrsin, S. 1970 Experiments on nearly homogeneous turbulent shear flow. *J. Fluid Mech.* **41**, 131–141.

Champagne, F. H., Sleicher, C. A. & Wehrmass, O. H. 1967 Turbulence measurements with inclined hot-wires. Parts 1 and 2. *J. Fluid Mech.* **28**, 153–193.

Clark, J. A. 1968 A study of incompressible turbulent boundary layers in channel flow. *J. Bas. Engng. Trans. A.S.M.E.* 68-FE-26.

Coantic, M. 1967 A study of turbulent pipe flow and of the structure of its viscous sublayer. *4th Euromech Colloquium.*

Coles, D. E. 1962 The turbulent boundary layer in a compressible fluid. *R.A.N.D. Rep.* 403–PR.

Collis, D. C. & Williams, M. J. 1959 Two-dimensional convection from heated wires at low Reynolds numbers. *J. Fluid Mech.* **6**, 357.

Comte-Bellot, G. 1965 Écoulement turbulent entre deux parois-parallèles. *Publ. Scientifiques et Techniques du Ministère de l'Air*, no. 419. Translated as *Aero. Res. Counc.* 31 609, FM4102 (1969).

Escudier, M. P. 1966 The turbulent incompressible hydrodynamic boundary layer. Ph.D. thesis, University of London.

Frenkiel, F. H. 1956 Effects of wire length in turbulence investigations with a hot wire anemometer. *Aeron. Quart.* **5**, 1–25.

Hanjalić, K. 1970 Two-dimensional asymmetric flow in ducts. Ph.D. thesis, University of London.

Hanjalić, K. & Launder, B. E. 1968 Fully-developed flow in rectangular ducts of non-uniform surface texture. Part I. An experimental investigation. *Imperial College, Dept. of Mech. Engng.* TWF/TN/48.

Hanratty, T. J. & Engen, J. M. 1957 *J. Am. Instn. Chem. Engrs.* **3**, 299.

Head, M. R. & Rechenberg, I. 1962 The Preston tube as a means of measuring skin friction. *J. Fluid Mech.* **14**, 1–17.

KJELLSTROM, B. & HEDBERG, S. 1968 Turbulence and shear stress measurements in a circular channel for testing of hot-wire anemometer measurements techniques and evaluation methods. *Aktiebolagat Atomenergi Rep.* RTL-1001.

KLEBANOFF, P. S. 1955 Characteristics of turbulence in a boundary layer with zero pressure gradient. *N.A.C.A. Rep.* 1247.

LAUFER, J. 1951 Investigation of turbulent flow in a two-dimensional channel. *N.A.C.A. Rep.* 1053.

LAUFER, J. 1954 The structure of turbulence in fully developed pipe flow. *N.A.C.A. Rep.* 1174.

LAWN, C. J. 1970 Application of the turbulence energy equation to fully developed flow in simple ducts. *C.E.G.B.* RD/B 1575.

MACMILLAN, F. A. 1954 Viscous effects on flattened Pitot tubes at low speeds. *J. Roy. Aero. Soc.* **58**, 837–9.

MACMILLAN, F. A. 1956 Experiments on Pitot tubes in shear flow. *Aero. Res. Counc. R. & M.* 3028.

MATHIEU, J. 1961 Contribution a l'étude aérothermique d'un jet plan évoluant en presence d'un paroi. *Publ. Scientifiques et Techniques du Ministère de l'Air*, no. 374.

PATEL, V. C. 1965 Calibration of the Preston tube and limitations on its use in pressure gradient. *J. Fluid Mech.* **23**, 185–208.

PERRY, A. E. & JOUBERT, P. N. 1963 Rough-wall boundary layers in adverse pressure gradients. *J. Fluids Mech.* **17**, 193–211.

TAILLAND, A. & MATHIEU, J. 1967 Jet pariétal. *J. Mécanique*, **6**, no. 1.

TOWNSEND, A. A. 1956 *The Structure of Turbulent Shear Flow.* Cambridge University Press.

VAN THINH, N. M. 1967 Sur le mesure de la vitesse dans un écoulement turbulent par anémometrie à fil chaud, au voisinage d'une paroi lisse. *C.R. Acad. Sci. Paris*, **264**, 1150–1152.

WILKIE, D., COWIN, M., BURNETT, P. & BURGOYNE, T. 1967 Friction factor measurements in a rectangular channel with walls of identical and non-identical roughness.

WYNGAARD, J. C. 1968 Measurements of small-scale turbulence structure with hot wires. *J. Scient. Instrum.* (*Phys. E.*) Ser. 2, **1**, 1105–1108.

ZARIĆ, Z. 1967 Turbulent heat transfer in a divergent convergent channel. *Jap. Soc. Mech. Engineers, Semi-Int. Symposium*, Tokyo.